Journal of the Mechanics and Physics of Solids 60 (2012) 750–783

Contents lists available at SciVerse ScienceDirect

Journal of the Mechanics and Physics of Solids

journal homepage: www.elsevier.com/locate/jmps

Modelling cell wall growth using a fibre-reinforced hyperelastic–viscoplastic constitutive law

R. Huang [a], A.A. Becker [b,*], I.A. Jones [b]

[a] Centre for Plant Integrative Biology, School of Biosciences, University of Nottingham, UK
[b] Department of Mechanical, Materials and Manufacturing Engineering, University of Nottingham, UK

ARTICLE INFO

Article history:
Received 4 April 2011
Received in revised form
29 July 2011
Accepted 3 December 2011
Available online 9 December 2011

Keywords:
Biological material
Fibre-reinforced composite
Viscoplastic material
Finite element method
Cell wall growth

ABSTRACT

A fibre-reinforced hyperelastic–viscoplastic model using a finite strain Finite Element (FE) analysis is presented to study the expansive growth of cell walls. Based on the connections between biological concepts and plasticity theory, e.g. wall-loosening and plastic yield, wall-stiffening and plastic hardening, the modelling of cell wall growth is established within a framework of anisotropic viscoplasticity aiming to represent the corresponding biology-controlled behaviour of a cell wall. In order to model *in vivo* growth, special attention is paid to the differences between a living cell and an isolated wall. The proposed hyperelastic–viscoplastic theory provides a unique framework to clarify the interplay between cellulose microfibrils and cell wall matrix and how this interplay regulates sustainable growth in a particular direction while maintaining the mechanical strength of the cell walls by new material deposition. Moreover, the effect of temperature is taken into account. A numerical scheme is suggested and FE case studies are presented and compared with experimental data.

1. Introduction

How cells expand despite the presence of the cell wall is a central issue in plant biology (Refregier et al., 2004). Animal and plant cells differ fundamentally with respect to their mode of cell enlargement. The typical cells in the animal body enlarge basically by an increase in plasma content in an isotonic environment. In contrast, the protoplasts of plant cells are encased in a rigid, elastically expandable cell wall infiltrated with water containing only moderate, osmotically negligible amounts of solutes (Schopfer, 2006). Wall synthesis without mechanical relaxation would only cause wall thickening without inducing the water uptake needed for wall extension and cell volume enlargement (Cosgrove, 1993a). To grow, plant cells must physically expand their restraining cell walls, while at the same time preserving the wall's mechanical integrity in the face of high turgor pressures. This is a delicate process that may be considered from many points of views (Cosgrove, 2000).

Lockhart (1965a,b) summarized a wide range of experimental data on wall extensibility in a formula that was readily comprehensive and became established as the well-known 'Lockhart equation'

$$r_g = \Phi(P-Y) \tag{1}$$

where r_g is the growth strain rate which is either positive for $P > Y$ or zero for $P \leq Y$, Φ is the extensibility of the cell wall, P is the turgor pressure, and Y is the yield threshold, i.e. the minimum pressure required for growth (Verbelen and

* Corresponding author. Tel.: +44 115 9513791.
E-mail address: a.a.becker@nottingham.ac.uk (A.A. Becker).

0022-5096
doi:10.1016/j.jmps.2011.12.003

Vissenberg, 2007). It appears that the threshold Y for plant tissues lies in the range of 0.2–0.4 MPa, and seems to be adjustable under some conditions (Cosgrove 1986). This simple Eq. (1) clearly states that the rate of cell expansion is a product of the imbalance between turgor pressure and the mechanical properties of the cell wall, emphasizing that the principal players are to be found in the symplast as well as in the apoplast (Verbelen and Vissenberg, 2007). Thus a central question is posed in developmental biology of plants: whether and how mechanical forces serve as cues for cellular behaviour (Dumais, 2007; Dumais and Steele, 2000; Hamant et al., 2008; Hamant and Traas, 2009; Steele, 2000). However, the Lockhart equation itself only provides a very limited answer to this question.

Although it has great merits for describing and measuring growth in physical terms, the Lockhart equation ignores the vectorial aspects of anisotropic growth and provides no hints with respect to the molecular changes in the wall properties (Schopfer, 2006). The long-term question of cell wall growth anisotropy is still waiting for a mechanical model handling anisotropic deformation (Baskin, 2005). Therefore, as a further development of the Lockhart model, multiscale constitutive modelling of cell wall anisotropic growth is a vital step to understand the role of mechanical forces in developmental biology and to develop predictable integrative models. However, although basic biomechanical frameworks of growth modelling have been discussed during recent decades in various fields, it is suggested that a universal mechanical growth law may not exist because the driving mechanism may be tissue dependent (Taber, 1995). Indeed, the growth constitutive law of cell wall depends on the unique characteristics of the wall structure and growth mechanisms.

It is widely accepted that the plant cell wall is considered to be a composite in which cellulose microfibrils are embedded into an amorphous matrix composed of hemicellulose, pectins and proteins. The composite must satisfy two contradictory requirements. It must be strong enough to resist the mechanical stress (which may exceed $10^8\,\mathrm{Nm}^{-2}$ (1000 bar)) generated by the cell turgor pressure and at the same time it must be sufficiently compliant to permit irreversible wall expansion. The cell wall accommodates these requirements through its composite structure, having stiff microfibrils with high mechanical strength in series with a viscoplastic amorphous matrix that moves in a controlled fashion (Cosgrove, 2001). Fig. 1 shows a schematic structure of a full anisotropic cell wall. The cellulose molecules form semi-crystalline microfibrils, several nanometres in width and many micrometres long, may be cross-linked by hemicelluloses molecules (McCann et al., 1990). Microfibrils have a tensile strength similar to that of steel, and are relatively inert and inextensible in growth (Iwamoto et al., 2009; Marga et al., 2005). The matrix consists of hemicelluloses with cross-linked microfibrils that form a load-bearing network, as well as pectins and proteins elaborated around the microfibril scaffold (Marga et al., 2005). Neighbouring microfibrils tend to be roughly parallel, giving the cell wall a mat-like appearance and a distinct structural anisotropy. Thus the cell wall can be modelled as a fully anisotropic composite

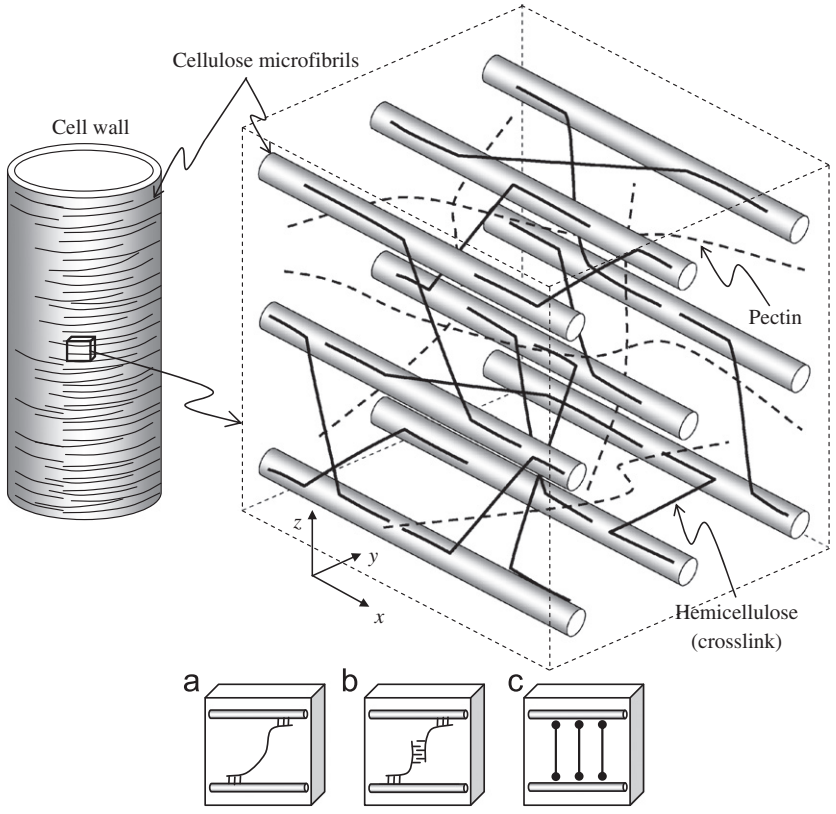

Fig. 1. Distribution of cellulose microfibrils and the cross-links in cell walls.

(Dumais et al., 2006) in which continuous microfibrils are aligned preferentially in one direction inside a representative element (see Fig. 1). It is noted that there exists a model based on the alternative assumption of discontinuous fibres (Burgert and Fratzl, 2007; Gao et al., 2003) which could account for (plastic) elongation of cell wall in the direction of the microfibrils. As the present work focuses on the cell wall without growth in the direction of the microfibrils, the hypothesis of continuous microfibrils is reasonable to characterise the role of microfibrils in anisotropic growth.

The structure of the hemicellulose cross-links between cellulose microfibrils is still an open question. Generally there are three different models: (a) the "tethered network" model, (b) the "multicoat" model, and (c) the "stratified cell wall" model as shown in Fig. 1 (Cosgrove, 2001; Burgert and Fratzl, 2007). In contrast to cellulose microfibrils which mainly play the role of load-bearing and are relatively inert in growth, the cross-links are connected with cell wall loosening which is the most crucial step in cell wall growth and the key to connect expansive growth with plasticity material models.

The wall loosening refers to the rearrangement of load-bearing cross-links which must occur in order to relax the wall stress and to allow polymer slippage as water is taken in and the wall expands irreversibly (Cosgrove, 1993b). In this interpretation, wall loosening is analogous to, and is referred to in the biological literature as (plastic) yielding. The irreversible expansion is therefore referred to as plastic deformation. Although the molecular details of wall loosening are largely unknown, there is convincing evidence that cells produce some kind of a wall-loosening factor that mediates a metabolically controlled chemo-rheological process facilitating the plastic deformation of the cell walls under the tensile force produced by turgor pressure (Schopfer, 2006). The idea of a wall loosening enzyme, e.g. enzymes which can break and transfer cross-links, is prevailing (Cosgrove, 1993b). This idea is analogous to the concept of crystal slip in plasticity, allowing the implementation of an equivalent plastic model of cell wall growth.

However, it is noted that, although a rough analogy exists between cell wall growth and metal plasticity, they differ from each other in the following three aspects. First, unlike metal plastic yielding models of in which the applied force (stress) is the *direct* driving force of yielding, turgor pressure on cell wall is appropriately termed a *passive* driving force for expansive growth in the limited sense that it provides the necessary mechanical force needed for wall yielding. There do not appear to be well established cases in which the yielding is mediated directly by a change in turgor pressure (Cosgrove, 1987). Instead, the regulatory aspects of cell growth appear to be controlled through changes in the cell wall properties which determine when walls shall become plastic and when they shall remain stable and rigid (Beckman, 1971).

Second, although irreversible expansive growth results from the breaking of bonds or cutting of cross-links in the cell wall matrix, it does not indicate that the matrix is irreversibly damaged (Proseus and Boyer, 2007). As a universal phenomenon, the living cell is able to self-recover (Keckes et al., 2003) or self-stabilise (Stamenovic and Ingber, 2009) under stress while regulating its behaviour using the stresses. This ability may be attributed to the molecular assembly (Cosgrove, 1997; Stamenovic and Ingber, 2009) which is one of the essential differences between cell wall growth and metal plasticity.

Third, the expansive growth of the cell surface by turgor pressure cannot proceed without the addition of new wall material because the cell wall would quickly become thinner and eventually rupture (Dumais et al., 2006). Wall loosening must therefore be accompanied by wall reinforcement in order to maintain the strength of the expansion. This requirement is generally satisfied by the synthesis of cellulose and other polysaccharides and their apposition to the inner surface of the wall (new material deposition). As much as 90–99% of the wall is new by the time the cell matures (Roberts, 1994). However, the incorporation of new materials in the growing wall can also downregulate growth by increasing wall stiffness (Schopfer, 2006). How the expansive growth integrates with wall deposition to generate a growth-sustaining activity is the key issue of mechanical modelling of *in vivo* cell growth since this is how the living cells essentially differ from the cell walls isolated from the necessary environment for growth (*isolated walls*) (Proseus and Boyer, 2006).

Therefore, the unique and essential quality of expansively growing cells ultimately lies in the yielding characteristics of the wall (Cosgrove, 1993b). The dynamic process of *in vivo* cell expansive growth depends on a balance of wall-loosening and wall-stiffening processes that can be independently regulated by different growth factors such as hormones and light (Schopfer, 2006). A proper mechanical model should adequately represent these constitutive responses which indicate an intrinsic connection between cell wall expansive growth and plasticity theory.

To develop the growth model in a framework of plasticity theory, it is worth looking back on the Lockhart model. Although it unveiled the viscoplastic behaviour of cell wall growth and has been extensively used in biological research, the Lockhart equation and its other modifications (see, e.g. Cosgrove, 1986; Geitmann and Ortega, 2009; Green et al., 1971; Ortega, 1990; Ray et al., 1972; Schopfer, 2006) cannot meet the requirement of more sophisticated analytical solutions or Finite Element (FE) numerical analysis, which essentially is due to the fact that the Lockhart model is a semi-empirical coordinate-dependent scalar equation rather than a frame-indifferent tensorial constitutive law.

To resolve the problem, some researchers suggested a tensor format of the original Lockhart equation or a thermodynamic modelling of polymer networks (see, e.g. Pietruszka, 2009; Veytsman and Cosgrove, 1998). Another method is to directly apply (elasto-visco) plasticity theory taking Lockhart equation as its consistent volumetric/uniaxial format. Boudaoud (2003) investigated the growth of isolated walled cells. The cells were modelled as elastic shells containing a liquid. Cell growth is driven by fluid pressure and is similar to a perfectly plastic deformation. Dumais et al. (2006) developed an anisotropic viscoplastic thin shell model of cell walls which was a first attempt at integrating mechanical deformation driven by turgor pressure and new material deposition. Application of their approach to the morphogenesis of tip-growing cells illustrates how the viscoplastic properties of the cell wall affect the shape of the cell.

Both plastic shell models laid down rigorous and inspiring frameworks for applying plasticity theory in cell wall growth. However, there are four important features missing in these models.

First, the mechanical role of cellulose microfibrils has not been introduced explicitly in these plastic models. In contrast to metal plastic deformation, growing cells grow in a particular direction while re-organizing themselves to the surroundings. It is widely accepted that cellulose microfibrils, the most pronounced structural unit of the cell wall, play a role as mechanical constraints which regulate the anisotropic growth (Bruce, 2003; Kerstens et al., 2001). This idea has been exploited in some fibre-reinforced elastic or viscous models. Hettiaratchi and O'callagham (1978) proposed a fibre-reinforced elastic model of cell walls assuming that the cell wall matrix can be characterised either by neo-Hookean or Mooney–Rivlin material models. The presence of microfibrils has been simulated by treating the matrix as being reinforced by thin inextensible cords. By using the analogy between plant cell and cardiac tissue, Chaplain (1993) suggested that the strain energy of plant cell walls has a similar form to that of a cardiac tissue in which microfibrils were treated as extensible. Recently, Dyson and Jensen (2010) suggested a fibre-reinforced viscous fluid model which considered the time-dependent behaviour of cell walls.

The coexistence of plastic models (without fibre-reinforcement) and fibre-reinforced elastic/viscous models actually indicates the complexity of cell wall growth. The plastic models emphasize the matrix-dominated mechanisms, e.g. wall loosening, which directly connect to bio-regulation of *in vivo* growth by enzymes. By contrast, fibre-reinforced elastic or viscous models pay attention to fibre-dominated mechanisms which reflect the role of stress equilibrium and kinematic compatibility in cell wall deformation mainly observed in *in vitro* experiments. Both kinds of mechanisms are reasonable and have their own supporting evidence from experimental data. From the point of view of integrative biology, fibre-reinforced elasto-viscoplastic model can unite the two kinds of mechanisms and can reconcile the existing models.

Second, the deposition of new material has not been considered in models based on plasticity theory. Dumais et al. (2006) treated the deposition by a kinematic assumption based on the fact that cell wall thickness of the tip of a root hair remains roughly constant during growth. This assumption bridged the gap between two different growth mechanisms, i.e. turgor-driven expansion and mass deposition, and was useful in application. However, for more general modelling, the assumption is too strict to represent the fact that the two mechanisms are essentially independent. Derbyshire et al. (2007) and Refregier et al. (2004) reported that the wall thickening by new material deposition was not always tightly coupled to the expansion. Proseus et al. (1999) reported elongation driven by rapid turgor pulses for which wall deposition was negligible. Moreover, from the point of view of phenomenological modelling, this observable assumption of thickness does not take into account the interplay between expansion and wall deposition at the molecular scale which can only be modelled by using internal variables. However, as the ideal-plastic model was used, internal variables were not been considered in the existing plastic models (Boudaoud, 2003; Dumais et al., 2006). A more general growth model should accommodate the wall expansion and wall deposition in a unified viscoplastic framework in which hardening parameters represent the interplay between different mechanisms to balance wall-loosening and wall-stiffening.

Third, the effect of temperature has not been discussed in the existing viscoplastic models. The yielding of cell wall, which is considered to be the key characteristics of growth, is regulated by enzymic mechanisms. Temperature has large effects on growth because the enzyme reactions involve chemical bonds having high activation energies (Proseus et al., 1999). A viscoplastic model taking account of temperature would be more useful for understanding growth and fitting experimental data.

Finally, finite strain theory was absent in the existing viscoplastic models. The cell wall may enlarge by 10 to 100 fold (Roberts, 1994) during expansive growth. Thus a growth model based on finite strain theory is required in the FE analysis. On the other hand, it is noted that several specific growth models were proposed in finite strain formats based on either the one-component continuum theory or the mixture theory (see e.g. Cowin, 2004; Garikipati et al., 2004; Maugin, 2011; Taber, 1995). The missing of a finite strain formulation of cell wall growth leaves a gap between the modelling of cell wall growth and the existing growth modelling in other fields, e.g. cardiac hypertrophy (Rodriguez et al., 1994).

In summary, cell wall growth reflects the complexity of integrative biology. The modelling should be based on a number of hypotheses to provide an improved understanding of the molecular interactions among cell wall polymers and the development of mechanics-based models to handle anisotropic growth (Baskin, 2005).

In the present work a fibre-reinforced hyperelastic–viscoplastic model with isotropic hardening is proposed using a finite strain formulation and implemented in the ABAQUS® FE computer code. The theory of strain invariants proposed by Gasser et al. (2006) for hyperelasticity and theory of stress invariants by Spencer (2001) for viscoplasticity are adopted and developed further for the fibre-reinforced growth model. The growth is treated as an anisotropic viscoplastic response and is formulated within the general framework suggested by Moran et al. (1990) and Simo and Hughes (1998).

In order to clarify the mechanisms of anisotropic growth of the cell wall, a decomposition of growth is suggested. The three parts of the growth, i.e. isochoric expansive growth, volumetric growth, and irreversible extension of microfibrils, are modelled independently in a consistent framework of viscoplasticity. Furthermore, to obtain an integrative growth model, the interplays between the isochoric expansive growth and the volumetric growth are discussed at two different scales, which lead to the mechanism-based hardening law at a molecular scale and the evolution equation of wall thickness at macroscopic scale. Based on the integrative constitutive model, an FE scheme is suggested to model the interplay among expansive growth, turgor pressure, and temperature. Numerical case studies are presented to illustrate that the suggested model can well represent some important characteristics of cell wall growth observed in experiments on *Chara* cell walls.

2. Kinematics of the model

2.1. Basic kinematics

At a certain initial time, the cell wall is represented as a continuum composite by its reference configuration, $\mathcal{B}_0$, with material points labelled by $\boldsymbol{X} \in \mathcal{B}_0$. At any current time, $t \in [0, +\infty)$, a mapping $\psi : \mathcal{B}_0 \to \mathcal{B}_t$ is a deformation which maps the reference configuration $\mathcal{B}_0$ onto the current configuration $\mathcal{B}_t$ embedded into Euclidean space $\mathbb{R}^3$. The current position of a material point $\boldsymbol{X}$ is written as $\boldsymbol{x} = \psi(\boldsymbol{X},t) \in \mathcal{B}_t \subset \mathbb{R}^3$. The deformation gradient is defined as $\boldsymbol{F}(\boldsymbol{X},t) = \partial\psi/\partial\boldsymbol{X}$ with its Jacobian denoted as $J = \det\boldsymbol{F} > 0$. In addition, the right and left Cauchy–Green tensors are defined, respectively, as (Marsden and Hughes, 1994)

$$\boldsymbol{C} = \boldsymbol{F}^T\boldsymbol{F}, \quad \boldsymbol{b} = \boldsymbol{F}\boldsymbol{F}^T. \tag{2}$$

To be consistent with the full anisotropic cell wall shown schematically in Fig. 1, it is assumed that there is a single family of microfibrils inside a representative element of cell wall. Therefore, resorting to the terminology of the Cosserat continuum (Marsden and Hughes, 1994), the local (averaged) kinematics of microfibrils can be represented by a deformation of an extensible *director* attached to a representative material point. In the reference configuration, the director is represented by a unit vector $\boldsymbol{a}_0(\boldsymbol{X}) \in \boldsymbol{S}^2$, where $\boldsymbol{S}^2$ is the unit sphere in $\mathbb{R}^3$, and is used to model vectors that are free to point in any direction (Marsden and Hughes, 1994). By using the perfect matrix–fibre bonding assumption (Gasser et al., 2006), at time t the director is mapped into its current configuration

$$\boldsymbol{a}(\boldsymbol{X},t) = \boldsymbol{F}(\boldsymbol{X},t)\boldsymbol{a}_0(\boldsymbol{X}) \in \mathbb{R}^3. \tag{3}$$

Thus the deformation gradient $\boldsymbol{F}$ suffices to define both the spatial direction

$$\tilde{\boldsymbol{a}} = \boldsymbol{a}/\sqrt{\lambda_{\boldsymbol{a}}}, \quad \tilde{\boldsymbol{a}}\cdot\tilde{\boldsymbol{a}} = 1 \tag{4}$$

and the extension (stretch) of the director

$$\lambda_{\boldsymbol{a}} = \boldsymbol{C} : \boldsymbol{A}_0 = \mathrm{tr}\boldsymbol{A} \tag{5}$$

where $\boldsymbol{A}_0 = \boldsymbol{a}_0 \otimes \boldsymbol{a}_0$ and $\boldsymbol{A} = \boldsymbol{a} \otimes \boldsymbol{a}$ with Cartesian components $(\boldsymbol{A}_0)_{IJ} = a_{0I}a_{0J}$ and $(\boldsymbol{A})_{ij} = a_i a_j$, respectively, are defined to be structural tensors of order two, symbols ':' and '$\otimes$' denote the double contraction of tensors and the vector product, respectively, and symbol 'tr' denotes the trace of tensor.

Therefore, the basic kinematics of model is described as the deformation $\psi : \mathcal{B}_0 \to \mathcal{B}_t$ mapping the pair of variables $(\boldsymbol{X},\boldsymbol{a}_0) \in \mathcal{B}_0 \times \boldsymbol{S}^2$ onto $(\boldsymbol{x},\boldsymbol{a}) \in \mathcal{B}_t \times \mathbb{R}^3$.

2.2. Multiplicative decomposition of the deformation gradient

Skalak (1981) pointed out that if the growth strains of each element of an originally unloaded and stress-free body are geometrically compatible, then the body remains *stress-free* after the growth occurs. If the growth strains are incompatible, however, internal (residual) stresses are generated. Chuong and Fung (1986a,b) used a nonlinear pseudo-elastic analysis to discuss the purpose of residual stress which may exist and undergo dynamic changes in biological tissues. Combining and extending the ideas of Skalak, Fung, and co-workers (Skalak, 1981; Chuong and Fung, 1986a,b; Fung, 1990), Rodriguez et al. (1994) suggested a kinematics model of *multiplicative decomposition* of the deformation gradient into the *mechanical* part and the *growth* part, just as employed in classical elasto-plasticity theory. By using Rodriguez's approach, the total deformation gradient, $\boldsymbol{F}$, can be decomposed as follows:

$$\boldsymbol{F} = \boldsymbol{F}^e\boldsymbol{F}^g. \tag{6}$$

Here tensor $\boldsymbol{F}^g$ is the deformation solely due to the growth of cell wall material, which is not constrained by surroundings and leaves the material in a zero-stress state. Tensor $\boldsymbol{F}^e$ is the accompanying elastic deformation that ensures the compatibility of the total growth deformation. This decomposition is analogous to the counterpart in phenomenological plasticity in which $\boldsymbol{F}^g$ represents the aggregate effect of dislocation motion and $\boldsymbol{F}^e$ the deformation caused by lattice distortion and rigid rotation of the lattice and material (Moran et al., 1990). Based on this analogy, some of the fundamental concepts, which are well established in classical plasticity theory based on the notion of an intermediate stress-free configuration (Simo and Hughes, 1998), can readily be applied to the field of not only mechanical modelling of growth, but also numerical analysis (Taber, 1995; Epstein and Maugin, 2000; Imatani and Maugin, 2002; Lubarda, 2004). This concept sheds new light on cell wall growth modelling and becomes the starting point of the present study.

Following plasticity theory, the decomposition in Eq. (6) leads to the notion of a (local) *intermediate configuration*, $\overline{\mathcal{B}}_t$, which consists of a collection of plastically deformed neighbourhoods defined by a pull-back $\boldsymbol{F}^{e-1}$ from $\mathcal{B}_t$ onto $\overline{\mathcal{B}}_t$ (see Fig. 2). From a phenomenological standpoint, one interprets $\boldsymbol{F}^{e-1}$ as the local deformation that releases the residual stress due to incompatibility of unconstrained growth from each neighbourhood on $\mathcal{B}_t$. Accordingly it is assumed that the local intermediate configuration $\overline{\mathcal{B}}_t$ is stress-free, which is consistent with the zero-stress state of unconstrained growth (Rodriguez et al., 1994; Taber, 1995).

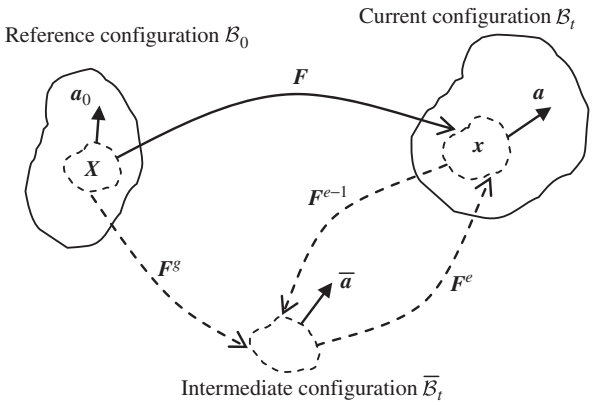

Fig. 2. Different geometric configurations and their relationships.

Using the standard conventions in continuum mechanics, the elastic right and left Cauchy–Green tensors are defined, respectively, as

$$\overline{\boldsymbol{C}} = \boldsymbol{F}^{eT}\boldsymbol{F}^{e}, \quad \overline{\boldsymbol{b}} = \boldsymbol{F}^{e}\boldsymbol{F}^{eT}. \tag{7}$$

Let $\boldsymbol{g}$ be the metric tensor on the current configuration $\mathcal{B}_t$. As $\mathcal{B}_t$ is embedded into Euclidean space $\mathbb{R}^3$, without loss in generality, let $\boldsymbol{g}=\boldsymbol{1}$ where $\boldsymbol{1}$ denotes the symmetric unit tensor with components δ_{ij}(δ_{ij} is Kronecker delta) in a Cartesian reference system. Thus the elastic right Cauchy–Green tensor $\overline{\boldsymbol{C}}$, which is interpreted as a tensor defined by pulling back the metric tensor $\boldsymbol{g}$ from $\mathcal{B}_t$ onto $\overline{\mathcal{B}}_t$, is the metric tensor on $\overline{\mathcal{B}}_t$.

Let $\boldsymbol{L}=\dot{\boldsymbol{F}}\boldsymbol{F}^{-1}$ be the spatial velocity gradient, where the symbol of superimposed dot denotes the material time derivative. By using the decomposition in Eq. (6), the decomposition of $\boldsymbol{L}$ is obtained as follows (Moran et al., 1990):

$$\boldsymbol{L} = \dot{\boldsymbol{F}}^{e}\boldsymbol{F}^{e-1} + \boldsymbol{F}^{e}\dot{\boldsymbol{F}}^{g}\boldsymbol{F}^{g-1}\boldsymbol{F}^{e-1} = \boldsymbol{L}^{e} + \boldsymbol{L}^{g}. \tag{8}$$

The symmetric parts of $\boldsymbol{L}^{e}$ and $\boldsymbol{L}^{g}$ are denoted, respectively, as

$$\boldsymbol{D}^{e} = (\boldsymbol{L}^{e} + \boldsymbol{L}^{eT})/2, \quad \boldsymbol{D}^{g} = (\boldsymbol{L}^{g} + \boldsymbol{L}^{gT})/2. \tag{9}$$

Eq. (9) leads to the decomposition of the rate of deformation tensor, $\boldsymbol{D}=\boldsymbol{D}^{e}+\boldsymbol{D}^{g}$, on $\mathcal{B}_t$.

Mapping $\boldsymbol{L}^{e}$ and $\boldsymbol{L}^{g}$ back to the intermediate configuration $\overline{\mathcal{B}}_t$, we obtain the elastic and growth parts of the velocity gradient on $\overline{\mathcal{B}}_t$, respectively, as

$$\overline{\boldsymbol{L}}^{e} = \boldsymbol{F}^{e-1}\dot{\boldsymbol{F}}^{e}, \quad \overline{\boldsymbol{L}}^{g} = \dot{\boldsymbol{F}}^{g}\boldsymbol{F}^{g-1}. \tag{10}$$

The elastic and growth rates of deformation tensors on $\overline{\mathcal{B}}_t$, denoted as $\overline{\boldsymbol{D}}^{e}$ and $\overline{\boldsymbol{D}}^{g}$, are defined by the symmetric parts of $\overline{\boldsymbol{L}}^{e}$ and $\overline{\boldsymbol{L}}^{g}$, respectively, as

$$\overline{\boldsymbol{D}}^{e} = \mathrm{sym}\overline{\boldsymbol{L}}^{e} = (\overline{\boldsymbol{C}}\overline{\boldsymbol{L}}^{e} + \overline{\boldsymbol{L}}^{eT}\overline{\boldsymbol{C}})/2, \quad \overline{\boldsymbol{D}}^{g} = \mathrm{sym}\overline{\boldsymbol{L}}^{g} = (\overline{\boldsymbol{C}}\overline{\boldsymbol{L}}^{g} + \overline{\boldsymbol{L}}^{gT}\overline{\boldsymbol{C}})/2. \tag{11}$$

Following the framework of plasticity theory, the elastic and viscoplastic responses of the growing cell wall can be formulated on the intermediate configuration separately.

3. Hyperelastic response

Proseus and Boyer (2006) suggested that there are two kinds of intermolecular bonds in a cell wall matrix; the strong bonds which are responsible for growth and are sensitive to temperature, and the weak bonds which are attributed to elastic extension and are not sensitive to temperature. This suggestion leads to the assumption that the elastic potential is unaffected by plastic flow (Moran et al., 1990) which provides the basis for the hyperelastic formulation on the intermediate configuration.

It is worth mentioning that, although the viscoplastic deformation, i.e. growth, is a finite deformation (wall enlarges by a factor from 10 to 100), the elastic strain is small (around 0.001) according to experimental observation (Proseus et al., 1999). If considering the order of magnitude of the elastic strain only, a linear constitutive law for small strain elasticity is good enough to represent the elastic response in cell wall. However, a constitutive model derived by combining a small elastic strain and a finite viscoplastic strain leads to a hypoelasto–viscoplasticity model which is inferior to the hyperelasto–viscoplasticty model in dealing with anisotropy and objectiveness (Belytschko et al., 2001).

By using hyperelasticity, the objectivity (Marsden and Hughes, 1994 p.8) of the elastic constitutive response is trivially satisfied (Simo and Ortiz, 1985). In addition, the hyperelastic–plastic formulation provides a natural framework for frame-indifferent formulation of anisotropic elasticity and anisotropic plastic yield (Belytschko et al., 2001). These features make hyperelasticity a natural choice for modelling the elastic response in anisotropic growth of cell wall. In the present study,

the strain invariants theory of fibre-reinforced hyperelastic model suggested by Gasser et al. (2006) is adopted for modelling elastic constitutive response on the intermediate configuration $\overline{\mathcal{B}}_t$.

As a metric tensor, $\overline{\boldsymbol{C}}$ is the fundamental strain tensor on $\overline{\mathcal{B}}_t$. The free energy, Ψ, which takes into account the specified distribution of cellulose microfibrils, is expressed solely in terms of $\overline{\boldsymbol{C}}$. A multiplicative decomposition (not to be confused with Rodriguez's kinematics) separates the *elastic* deformation gradient $\boldsymbol{F}^e$ into volume-changing (dilational) and volume-preserving (distortional) parts. The strain measure of the dilational part is a Jacobian $\bar{J}=\det\boldsymbol{F}^e$. On the other hand, the strain measures of the distortional part are the modified elastic right and left Cauchy–Green tensors, $\hat{\overline{\boldsymbol{C}}}$ and $\hat{\overline{\boldsymbol{b}}}$, defined as

$$\hat{\overline{\boldsymbol{C}}}=\bar{J}^{-2/3}\overline{\boldsymbol{C}},\quad \hat{\overline{\boldsymbol{b}}}=\bar{J}^{-2/3}\overline{\boldsymbol{b}} \tag{12}$$

which satisfy the conditions $\det\hat{\overline{\boldsymbol{C}}}=\det\hat{\overline{\boldsymbol{b}}}=1$.

Based on the experimental observations of biological tissues, a decoupled representation of the free energy function, Ψ, which describes separately the volumetric and isochoric contributions, was suggested by Gasser et al. (2006). The general form of this decoupled representation of Ψ is presented on the intermediate configuration as follows:

$$\Psi(\bar{J},\hat{\overline{\boldsymbol{C}}},\overline{\boldsymbol{A}})=\Psi_{vol}(\bar{J})+\Psi_{iso}(\hat{\bar{I}}_1,\hat{\bar{I}}_2,\hat{\bar{I}}_4,\hat{\bar{I}}_5) \tag{13}$$

where $\overline{\boldsymbol{A}}=\overline{\boldsymbol{a}}\otimes\overline{\boldsymbol{a}}$ in which the vector $\overline{\boldsymbol{a}}$ is defined by

$$\overline{\boldsymbol{a}}=\boldsymbol{F}^g\boldsymbol{a}_0, \tag{14}$$

the four invariants $\hat{\bar{I}}_1,\hat{\bar{I}}_2,\hat{\bar{I}}_4,\hat{\bar{I}}_5$ are defined as

$$\hat{\bar{I}}_1(\hat{\overline{\boldsymbol{C}}})=\mathrm{tr}\hat{\overline{\boldsymbol{C}}},\quad \hat{\bar{I}}_2(\hat{\overline{\boldsymbol{C}}})=\tfrac{1}{2}\left[(\mathrm{tr}\hat{\overline{\boldsymbol{C}}})^2-\mathrm{tr}\hat{\overline{\boldsymbol{C}}}^2\right],\quad \hat{\bar{I}}_4(\hat{\overline{\boldsymbol{C}}},\overline{\boldsymbol{A}})=\hat{\overline{\boldsymbol{C}}}:\overline{\boldsymbol{A}}=\hat{\lambda}_{\overline{\boldsymbol{a}}},\quad \hat{\bar{I}}_5(\hat{\overline{\boldsymbol{C}}},\overline{\boldsymbol{A}})=\hat{\overline{\boldsymbol{C}}}^2:\overline{\boldsymbol{A}}. \tag{15}$$

In the present modelling of cell wall, a particular neo-Hookean free energy function (Gasser et al., 2006) is used as follows:

$$\Psi(\bar{J},\hat{\overline{\boldsymbol{C}}},\overline{\boldsymbol{A}})=\Psi_{vol}(\bar{J})+\Psi_{iso}(\hat{\bar{I}}_1,\hat{\bar{I}}_4)=\frac{1}{2}\kappa(\bar{J}-1)^2+\frac{1}{2}\mu(\hat{\bar{I}}_1-3)+\frac{1}{2}\frac{\kappa_1}{\kappa_2}\left[\exp(\kappa_2(\hat{\bar{I}}_4-1)^2)-1\right] \tag{16}$$

where κ and μ are interpreted as the bulk modulus and shear modulus of cell wall matrix, respectively, and κ_1 and κ_2 are parameters of the elastic response of cellulose microfibrils. The first and second terms on the right side of Eq. (16) define the isotropic hyperelastic response of cell wall matrix. The third term is obtained from a more general formulation suggested in Gasser et al. (2006) by specifying the distribution of fibres.

The second Piola–Kirchhoff stress $\overline{\boldsymbol{S}}$ and elastic tangent modulus $\overline{\mathbb{C}}$ on the intermediate configuration can be calculated by the hyperelastic relationships

$$\overline{\boldsymbol{S}}=2\frac{\partial\Psi(\bar{J},\hat{\overline{\boldsymbol{C}}},\overline{\boldsymbol{A}})}{\partial\overline{\boldsymbol{C}}} \tag{17}$$

and

$$\overline{\mathbb{C}}=4\frac{\partial^2\Psi(\bar{J},\hat{\overline{\boldsymbol{C}}},\overline{\boldsymbol{A}})}{\partial\overline{\boldsymbol{C}}\partial\overline{\boldsymbol{C}}} \tag{18}$$

respectively. Eq. (17) is the constitutive equation of hyperelasticity on $\overline{\mathcal{B}}_t$. In addition, with the elastic tangent modulus $\overline{\mathbb{C}}$, the corresponding rate constitutive equation is defined as $\dot{\overline{\boldsymbol{S}}}=\overline{\mathbb{C}}:\overline{\boldsymbol{D}}^e$.

By using $\overline{\mathbf{S}}$ and $\overline{\mathbb{C}}$, the Cauchy stress tensor σ and elastic tangent modulus $\mathfrak{c}$ on the current configuration $\mathcal{B}_t$ are calculated by pushing $\overline{\mathbf{S}}$ and $\overline{\mathbb{C}}$ forward from $\overline{\mathcal{B}}_t$ to $\mathcal{B}_t$, respectively, as follows:

$$\boldsymbol{\sigma}=\bar{J}^{-1}\boldsymbol{F}^e\overline{\mathbf{S}}\boldsymbol{F}^{eT} \tag{19}$$

and

$$[\mathfrak{c}]_{ijkl}=\bar{J}^{-1}F^e_{iI}F^e_{jJ}F^e_{kK}F^e_{lL}[\overline{\mathbb{C}}]_{IJKL}. \tag{20}$$

Eq. (19) is the constitutive equation of hyperelasticity on $\mathcal{B}_t$, and the corresponding rate constitutive equation is defined as $L^e_v\boldsymbol{\tau}=\mathfrak{c}:\boldsymbol{D}^e$ in which $\boldsymbol{\tau}=\bar{J}\boldsymbol{\sigma}$ is the Kirchhoff stress tensor and $L^e_v\boldsymbol{\tau}$, which is the push-forward of $\dot{\overline{\boldsymbol{S}}}$ by $\boldsymbol{F}^e$ (i.e. $L^e_v\boldsymbol{\tau}=\boldsymbol{F}^e\dot{\overline{\boldsymbol{S}}}\boldsymbol{F}^{eT}$), is the elastic Lie derivative of the Kirchhoff stress defined as $L^e_v\boldsymbol{\tau}=\dot{\boldsymbol{\tau}}-\boldsymbol{L}^e\boldsymbol{\tau}-\boldsymbol{\tau}\boldsymbol{L}^{eT}$ (Marsden and Hughes, 1994; Belytschko et al., 2001).

The explicit expressions of $\overline{\boldsymbol{S}}$, $\overline{\mathbb{C}}$, $\boldsymbol{\sigma}$ and $\mathfrak{c}$ calculated from the specified free energy in Eq. (16) are shown in Table 1. The calculation of the expressions of $\overline{\boldsymbol{S}}$ and $\overline{\mathbb{C}}$ involves the derivatives of J, $\hat{\overline{\boldsymbol{C}}}$ and $\overline{\boldsymbol{C}}^{-1}$ with respect to $\overline{\boldsymbol{C}}$. For completeness, these expressions are given as follows (Simo and Hughes, 1998; Gasser et al., 2006):

$$\frac{\partial\bar{J}}{\partial\overline{\boldsymbol{C}}}=\frac{1}{2}\bar{J}\overline{\boldsymbol{C}}^{-1}, \tag{21}$$

$$\frac{\partial\hat{\overline{\boldsymbol{C}}}}{\partial\overline{\boldsymbol{C}}}=\frac{1}{2}\bar{J}^{-2/3}\left[\mathbb{I}-\frac{1}{3}\overline{\boldsymbol{C}}\otimes\overline{\boldsymbol{C}}^{-1}\right] \tag{22}$$

Table 1
Stress tensor and elastic tangent modulus.

Intermediate configuration description	Spatial description
Second Piola–Kirchhoff stress tensor $\overline{\boldsymbol{S}}=\kappa\bar{J}(\bar{J}-1)\overline{\boldsymbol{C}}^{-1}+\mu\bar{J}^{-2/3}\mathrm{DEV}[\boldsymbol{1}]$ $+2\kappa_1\alpha_1\bar{J}^{-2/3}\mathrm{DEV}\left[\overline{\boldsymbol{A}}\right]$	Cauchy stress tensor $\boldsymbol{\sigma}=\kappa(\bar{J}-1)\boldsymbol{1}+\mu\bar{J}^{-1}\mathrm{dev}[\hat{\bar{\boldsymbol{b}}}]$ $+2\kappa_1\alpha_1\bar{J}^{-5/3}\mathrm{dev}[\boldsymbol{A}]$
Elastic tangent modulus $\overline{\mathbb{C}}=\kappa\bar{J}(2\bar{J}-1)(\overline{\boldsymbol{C}}^{-1}\otimes\overline{\boldsymbol{C}}^{-1})-2\kappa\bar{J}(\bar{J}-1)\mathbb{I}_{\overline{\boldsymbol{C}}^{-1}}$ $+\frac{2}{3}\mu\bar{J}^{-2/3}\left\{(\mathrm{tr}\overline{\boldsymbol{C}})\left[\mathbb{I}_{\overline{\boldsymbol{C}}^{-1}}-\frac{1}{3}\overline{\boldsymbol{C}}^{-1}\otimes\overline{\boldsymbol{C}}^{-1}\right]\right.$ $\left.-[\overline{\boldsymbol{C}}^{-1}\otimes\mathrm{DEV}[\boldsymbol{1}]+\mathrm{DEV}[\boldsymbol{1}]\otimes\overline{\boldsymbol{C}}^{-1}]\right\}$ $+2\kappa_1\bar{J}^{-4/3}\left\{\alpha_2\mathrm{DEV}\left[\overline{\boldsymbol{A}}\right]\otimes\mathrm{DEV}\left[\overline{\boldsymbol{A}}\right]\right.$ $+\frac{1}{3}\alpha_1\hat{\lambda}_{\overline{\boldsymbol{a}}}\bar{J}^{-4/3}\left[\mathbb{I}_{\overline{\boldsymbol{C}}^{-1}}-\frac{1}{3}\overline{\boldsymbol{C}}^{-1}\otimes\overline{\boldsymbol{C}}^{-1}\right]$ $\left.-\frac{1}{3}\alpha_1\bar{J}^{2/3}\left[\overline{\boldsymbol{C}}^{-1}\otimes\mathrm{DEV}\left[\overline{\boldsymbol{A}}\right]+\mathrm{DEV}\left[\overline{\boldsymbol{A}}\right]\otimes\overline{\boldsymbol{C}}^{-1}\right]\right\}$	Elastic tangent modulus $\mathfrak{c}=\kappa(2\bar{J}-1)(\boldsymbol{1}\otimes\boldsymbol{1})-2\kappa(\bar{J}-1)\mathbb{I}$ $+\frac{2}{3}\mu\bar{J}^{-1}\left\{\mathrm{tr}\hat{\bar{\boldsymbol{b}}}\left[\mathbb{I}-\frac{1}{3}\boldsymbol{1}\otimes\boldsymbol{1}\right]\right.$ $\left.-[\boldsymbol{1}\otimes\mathrm{dev}[\hat{\bar{\boldsymbol{b}}}]+\mathrm{dev}[\hat{\bar{\boldsymbol{b}}}]\otimes\boldsymbol{1}]\right\}$ $+2\kappa_1\bar{J}^{-7/3}\left\{\alpha_2\mathrm{dev}[\boldsymbol{A}]\otimes\mathrm{dev}[\boldsymbol{A}]\right.$ $+\frac{1}{3}\alpha_1\hat{\lambda}_{\overline{\boldsymbol{a}}}\bar{J}^{4/3}\left[\mathbb{I}-\frac{1}{3}\boldsymbol{1}\otimes\boldsymbol{1}\right]$ $\left.-\frac{1}{3}\alpha_1\bar{J}^{2/3}\left[\boldsymbol{1}\otimes\mathrm{dev}[\boldsymbol{A}]+\mathrm{dev}[\boldsymbol{A}]\otimes\boldsymbol{1}\right]\right\}$

in which $\mathbb{I}$ is the fourth-order unit tensor with components $(\mathbb{I})_{IJKL}=\frac{1}{2}(\delta_{IJ}\delta_{KL}+\delta_{IK}\delta_{JL})$, and

$$\left(\frac{\partial\overline{\boldsymbol{C}}^{-1}}{\partial\overline{\boldsymbol{C}}}\right)_{IJKL}=-(\mathbb{I}_{\overline{\boldsymbol{C}}^{-1}})_{IJKL}=-(\overline{C}^{-1}_{IK}\overline{C}^{-1}_{JL}+\overline{C}^{-1}_{IL}\overline{C}^{-1}_{JK})/2. \tag{23}$$

In Table 1, two deviatoric operators, DEV[·] on $\overline{\mathcal{B}}_t$ and dev[·] on $\mathcal{B}_t$, are defined, respectively, as

$$\mathrm{DEV}[\cdot]=(\cdot)-\tfrac{1}{3}\mathrm{Tr}(\cdot)\overline{\boldsymbol{C}}^{-1},\quad \mathrm{dev}[\cdot]=(\cdot)-\tfrac{1}{3}\mathrm{tr}(\cdot)\boldsymbol{1}. \tag{24}$$

Whereby the function Tr(·) is defined on $\overline{\mathcal{B}}_t$ as $\mathrm{Tr}(\cdot)=\overline{\boldsymbol{C}}:(\cdot)$ which is the counterpart of $\mathrm{tr}(\cdot)=\boldsymbol{1}:(\cdot)$ on $\mathcal{B}_t$. Also in Table 1, the two coefficients α_1 and α_2 are defined as follows:

$$\alpha_1=(\hat{\lambda}_{\overline{\boldsymbol{a}}}-1)\exp(\kappa_2(\hat{\lambda}_{\overline{\boldsymbol{a}}}-1)^2),\quad \alpha_2=(1+2\kappa_2(\hat{\lambda}_{\overline{\boldsymbol{a}}}-1)^2)\exp(\kappa_2(\hat{\lambda}_{\overline{\boldsymbol{a}}}-1)^2). \tag{25}$$

4. Viscoplastic response (growth)

The Lockhart model represented a milestone in the modelling of cell wall growth. However, as pointed out in the preceding discussion, the Lockhart equation and its variations were not presented in the tensorial format and implicitly or explicitly depended on a *priori* global coordinate coinciding with a longitudinal axis along which the cell wall elongates. In order to develop a frame-indifferent viscoplastic constitutive response consistent with the Lockhart equation and its interpretation, our intention is to develop an anisotropic viscoplastic formulation based on invariants of stress tensors for which the *local* direction of microfibrils is the only particular direction it needs. Moreover, the mechanisms of growth at the molecular scale are taken into account to present a growth model which distinguishes living cells from isolated walls even without explicitly using biological variables.

The strategy for obtaining an integrative growth model is outlined as follows. First a decomposition of growth is suggested to characterise the three parts of the growth (isochoric expansive growth, volumetric growth and irreversible microfibrils extension) and to identify the corresponding driving forces. Second, the three parts of the growth are modelled in a consistent framework of viscoplasticity to obtain their yield functions and flow rules. Third, the interplays between different parts of the growth at both the molecular scale and the macroscopic scale are studied to obtain the hardening law and evolution of cell wall thickness. Finally, a numerical scheme for application to the integrative growth model is suggested.

4.1. Decomposition of growth and the driving forces of growth

To account for the growth anisotropy, it was proposed that cells have independent growth mechanisms in different principal directions (Baskin, 2005). Two hypotheses, namely turgor driven creep and new material deposition, are widely accepted to be the fundamental aspects of the anisotropic cell wall growth. Based on these hypotheses, it is assumed that the growth of cell walls refers to three independent mechanisms.

First, Fig. 3(a) schematically shows the mechanism of the turgor-driven creep (isochoric expansive growth) by using a tethered network model. During the first extension, shear forces build up in the hydrogen bonds between the microfibrils and the cross-links, due to their different modulus of elasticity (Piggott, 1980). On the other hand, tensions accumulate in

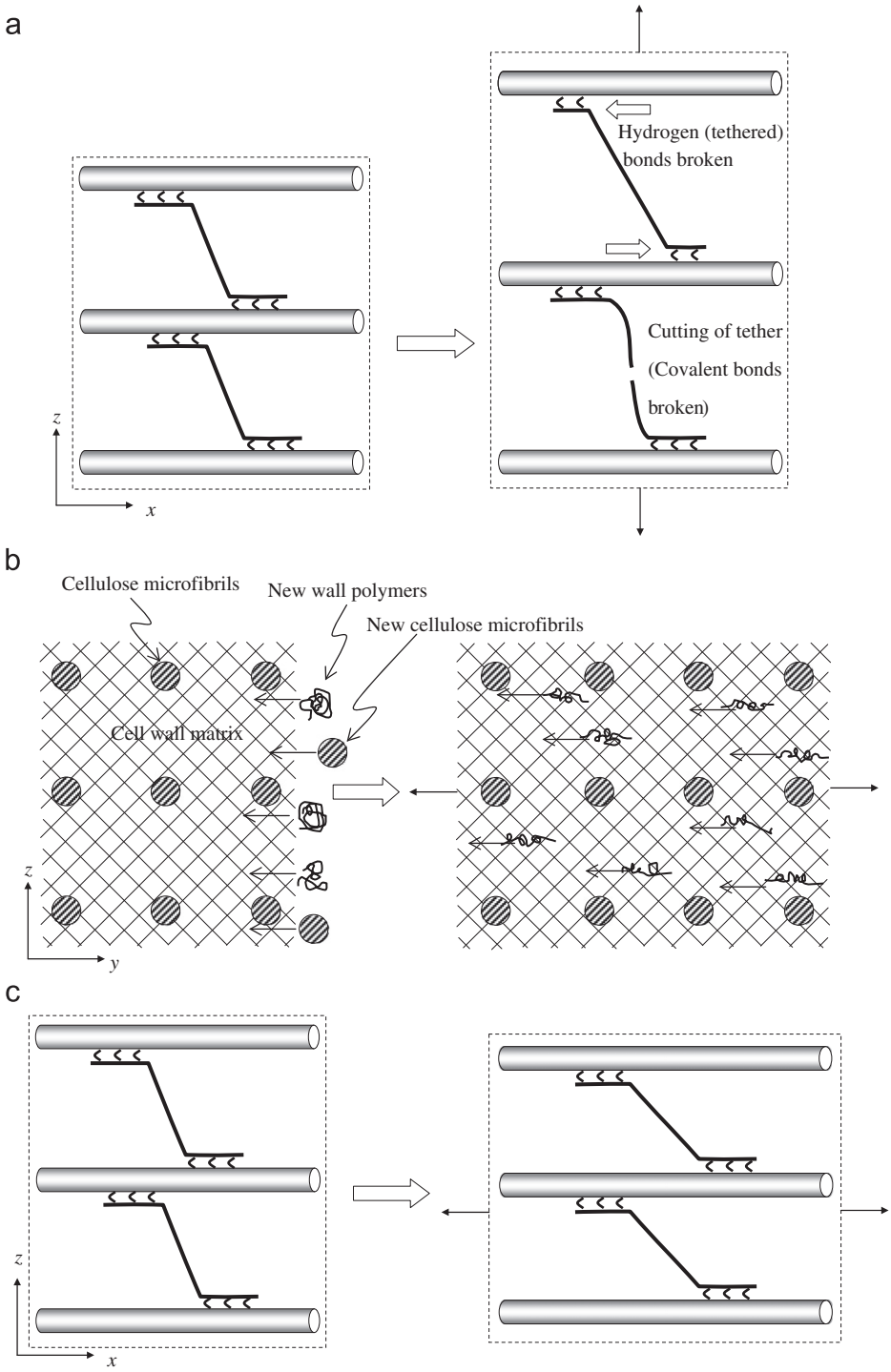

Fig. 3. Growth mechanisms of cell wall (a) isochoric expansive growth without irreversible microfibrils extension driven by Spencer's deviatoric stress where covalent bonds and hydrogen bonds are broken. (b)Volumetric growth without irreversible microfibrils extension driven by the stress regulating the deformation of the new wall polymers and (c) irreversible microfibrils extension driven by the tension of microfibrils.

the tethers. Above a certain 'yield' point, the shear forces and tensions can passively cause the irreversible loosening of the tethering network by the enzymatic breaking of the hydrogen bonds and cutting of the tethers (Proseus et al., 1999). The microfibrils can slide along each other and the matrix undergoes plastic deformation (Spatz et al., 1999; Kerstens et al., 2001). Neither plastic volumetric deformation nor irreversible microfibrils extension takes place in this process. This mechanism dominates the wall surface expansion and longitudinal elongation.

Second, a plastic volumetric deformation is introduced to address the new material deposition. As reported by Proseus and Boyer (2005), the cell wall can be considered as a porous material and turgor pressure P regulates the deposition of new wall polymers via a mechanism of concentration and turgor-induced deformation of the polymers themselves instead of wall matrix as illustrated in Fig. 3(b). Moreover, it is noted that isochoric expansion does not account for this polymer deposition (Proseus and Boyer, 2005). A precise model of new material deposition should take account of the flux of new mass through wall surface along the wall thickness direction. However, such a model leads to the so-called second-order model of volumetric growth involving the strain gradient (Epstein and Maugin, 2000). Due to the fact that the characteristic dimension of the wall thickness is far smaller than the characteristic dimensions in other directions, we model the new material deposition as a process in which the new wall material is produced by a smooth volumetric source of mass, m_V, inside $\mathcal{B}_t$ instead of a mass flux through the boundary of $\mathcal{B}_t$. The mass balance law on $\mathcal{B}_t$ is (Epstein and Maugin, 2000)

$$\frac{D\rho}{Dt} = m_V - \rho \mathrm{tr}\boldsymbol{D} \tag{26}$$

where ρ is the mass density on the current configuration, $D(\cdot)/Dt$ is the material time derivative. By using the additive decomposition of the rate of deformation tensor, Eq. (26) is assumed to be separable into two equations as follows:

$$\frac{1}{\rho}\frac{D\rho}{Dt} = -\mathrm{tr}\boldsymbol{D}^e, \quad \frac{m_V}{\rho} = \mathrm{tr}\boldsymbol{D}^g. \tag{27}$$

Eq. (27) means that new wall material of the same density ρ is deposited on the current cell wall during growth. In other words, growth does not take place at the expense of porosity (Epstein and Maugin, 2000). By assuming ρ is constant in time and position, Eq. (27) is identical to the well-known formulation of rate of volumetric growth, $\partial V/\partial t = V\mathrm{tr}\boldsymbol{D}^g$, where V is a growth volume (Rodriguez et al., 1994; Taber, 1995). Thus the new material deposition is represented by a plastic volumetric deformation. No plastic microfibrils extension takes place in this volumetric deformation process. This growth mechanism dominates the thickness of cell wall.

Third, to complete the decomposition of growth, it is assumed that microfibrils can undergo plastic extension under tension without volumetric deformation as shown in Fig. 3(c). The microfibrils extension dominates the circumferential deformation.

Thus a *decomposition of growth* is assumed here and growth can be decomposed into three parts: isochoric expansive growth without irreversible microfibrils extension (part I), volumetric growth without irreversible microfibrils extension (part II), and irreversible microfibrils extension without volumetric change (part III). As the three parts of the growth are based on different mechanisms, the stress tensor is decomposed into the corresponding driving forces accordingly.

We start from the relatively simple driving force of part III of the growth. A tensor $\boldsymbol{R}_{\lambda_a}$, interpreted as an admissible rate of deformation tensor on $\mathcal{B}_t$, is introduced as

$$\boldsymbol{R}_{\lambda_a} = \mathrm{dev}[\tilde{\boldsymbol{A}}] \tag{28}$$

where $\tilde{\boldsymbol{A}} = \tilde{\boldsymbol{a}} \otimes \tilde{\boldsymbol{a}}$. By using a pull-back mapping $\boldsymbol{F}^{eT}(\cdot)\boldsymbol{F}^e$ for the rate of deformation tensor, $\boldsymbol{R}_{\lambda_a}$ is mapped onto $\overline{\mathcal{B}}_t$ as

$$\overline{\boldsymbol{R}}_{\lambda_a} = \hat{\boldsymbol{A}} - \tfrac{1}{3}\overline{\boldsymbol{C}} \tag{29}$$

where $\hat{\boldsymbol{A}} = \boldsymbol{F}^{eT}\tilde{\boldsymbol{A}}\boldsymbol{F}^e$. It can be proved that tensor $\boldsymbol{R}_{\lambda_a}$ satisfies the condition $\mathrm{tr}\boldsymbol{R}_{\lambda_a} = 0$. Thus tensor $\boldsymbol{R}_{\lambda_a}$ (or $\overline{\boldsymbol{R}}_{\lambda_a}$) is the admissible plastic flow direction for part III of the growth. The corresponding *effective* driving force are defined as the stress powers per unit reference volume

$$\tau_{\lambda_a}(\boldsymbol{\tau}) = \boldsymbol{\tau} : \boldsymbol{R}_{\lambda_a} \equiv \overline{\boldsymbol{S}} : \overline{\boldsymbol{R}}_{\lambda_a} = \overline{\tau}_{\lambda_a}(\overline{\boldsymbol{S}}). \tag{30}$$

Then the corresponding driving force tensor is defined on $\mathcal{B}_t$ as

$$\boldsymbol{\tau}_{\lambda_a} = \tau_{\lambda_a}\tilde{\boldsymbol{A}} \tag{31}$$

or equivalently on $\overline{\mathcal{B}}_t$ as

$$\overline{\boldsymbol{S}}_{\lambda_a} = \frac{\overline{\tau}_{\lambda_a}}{\lambda_a}\overline{\boldsymbol{A}} \tag{32}$$

by mapping $\boldsymbol{\tau}_{\lambda_a}$ back onto $\overline{\mathcal{B}}_t$.

To obtain the expression for the driving force of part II of the growth, a spatial stress tensor $\boldsymbol{\tau}^A$ (or $\overline{\boldsymbol{S}}^A$ equivalently on $\overline{\mathcal{B}}_t$) is introduced as

$$\boldsymbol{\tau}^A = \boldsymbol{\tau} - \left\{\boldsymbol{\tau} : \tilde{\boldsymbol{A}}\right\}\tilde{\boldsymbol{A}}, \quad \overline{\boldsymbol{S}}^A = \overline{\boldsymbol{S}} - \frac{1}{\lambda_a^2}\|\overline{\boldsymbol{S}}\|_{\overline{\boldsymbol{a}}}\overline{\boldsymbol{A}} \tag{33}$$

where the function $\|(\cdot)\|_{\overline{\boldsymbol{a}}}$ is defined on $\overline{\mathcal{B}}_t$ as

$$\|(\cdot)\|_{\overline{\boldsymbol{a}}} = [\overline{\boldsymbol{C}}(\cdot)\overline{\boldsymbol{C}}] : \overline{\boldsymbol{A}}. \tag{34}$$

The corresponding *effective* driving force is defined as

$$\tau_{vol}(\boldsymbol{\tau}) = \mathrm{tr}\boldsymbol{\tau}^A \equiv \mathrm{Tr}\overline{\boldsymbol{S}}^A = \overline{\tau}_{vol}(\overline{\boldsymbol{S}}) \tag{35}$$

for part II of the growth. The meaning of this driving force is clear when the corresponding flow rule is obtained (see Eqs. (72) and (74)). Then the corresponding tensor of driving force is defined on $\mathcal{B}_t$ as

$$\boldsymbol{\tau}_{vol} = \tfrac{1}{3}\tau_{vol}\boldsymbol{1} \tag{36}$$

or equivalently on $\overline{\mathcal{B}}_t$ as

$$\overline{\boldsymbol{S}}_{vol} = \tfrac{1}{3}\overline{\tau}_{vol}\overline{\boldsymbol{C}}^{-1}. \tag{37}$$

Once tensors $\boldsymbol{\tau}_{vol}$ and $\boldsymbol{\tau}_{\lambda_{\boldsymbol{a}}}$(or $\overline{\boldsymbol{S}}_{vol}$ and $\overline{\boldsymbol{S}}_{\lambda_{\boldsymbol{a}}}$) are obtained, the driving force of part I of the growth is defined as

$$\boldsymbol{\tau}^{dev} = \boldsymbol{\tau} - \tfrac{3}{2}\left[\boldsymbol{\tau}_{vol} + \boldsymbol{\tau}_{\lambda_{\boldsymbol{a}}}\right] = \boldsymbol{\tau} - \tfrac{1}{2}\left[\left\{\mathrm{tr}\boldsymbol{\tau}^A\right\}\boldsymbol{1} + 3\left\{\boldsymbol{\tau} : \boldsymbol{R}_{\lambda_{\boldsymbol{a}}}\right\}\tilde{\boldsymbol{A}}\right] \tag{38}$$

on $\mathcal{B}_t$ or equivalently as

$$\overline{\boldsymbol{S}}^{DEV} = \overline{\boldsymbol{S}} - \frac{3}{2}\left[\overline{\boldsymbol{S}}_{vol} + \overline{\boldsymbol{S}}_{\lambda_{\boldsymbol{a}}}\right] = \overline{\boldsymbol{S}} - \frac{1}{2}\left[\left\{\mathrm{Tr}\overline{\boldsymbol{S}}^A\right\}\overline{\boldsymbol{C}}^{-1} + \frac{3}{\lambda_{\boldsymbol{a}}}\left\{\overline{\boldsymbol{S}} : \overline{\boldsymbol{R}}_{\lambda_{\boldsymbol{a}}}\right\}\overline{\boldsymbol{A}}\right] \tag{39}$$

on $\overline{\mathcal{B}}_t$. It is straightforward to prove that the spatial stress tensor $\boldsymbol{\tau}^{dev}$ satisfies the conditions

$$\boldsymbol{\tau}^{dev} : \boldsymbol{A} = 0, \quad \mathrm{tr}\boldsymbol{\tau}^{dev} = 0. \tag{40}$$

Equivalently, the stress tensor $\overline{\boldsymbol{S}}^{DEV}$ on the intermediate configuration satisfies the conditions

$$\|\overline{\boldsymbol{S}}^{DEV}\|_{\overline{\boldsymbol{a}}} = 0, \quad \mathrm{Tr}\overline{\boldsymbol{S}}^{DEV} = 0. \tag{41}$$

Eqs. (40) and (41) indicate that stress tensor $\boldsymbol{\tau}^{dev}$ or $\overline{\boldsymbol{S}}^{DEV}$ is the driving force of part III of the growth because neither plastic volumetric deformation nor irreversible microfibrils extension takes place under this driving force. It is noted that the tensor $\boldsymbol{\tau}^{dev}$ is exactly the same as the deviatoric stress tensor suggested by Spencer (2001) in infinitesimal strain format restricted to a composite containing a single family of microfibrils. Here Spencer's formulation is extended into a finite strain model. For convenience, $\boldsymbol{\tau}^{dev}$ and $\overline{\boldsymbol{S}}^{DEV}$ are referred to as Spencer's deviatoric stress tensors on $\mathcal{B}_t$ and $\overline{\mathcal{B}}_t$, respectively.

Hitherto, a set of stress tensors, $\boldsymbol{\tau}^{dev}$, $\boldsymbol{\tau}_{vol}$ and $\boldsymbol{\tau}_{\lambda_{\boldsymbol{a}}}$ on $\mathcal{B}_t$ (or $\overline{\boldsymbol{S}}^{DEV}$, $\overline{\boldsymbol{S}}_{vol}$ and $\overline{\boldsymbol{S}}_{\lambda_{\boldsymbol{a}}}$ on $\overline{\mathcal{B}}_t$), is obtained as the set of driving forces of cell wall growth corresponding to the decomposition of growth. These stress tensors play a similar role as the standard deviatoric stress tensor, dev[$\boldsymbol{\sigma}$], in the J_2-viscoplasticity theory and are the fundamental tensors for establishing the yield criterion and plastic flow rule.

4.2. Yield criterion

Due to their independent growth mechanisms, the three parts of the growth, i.e. isochoric expansive growth, volumetric growth and irreversible microfibrils extension, have their own yield functions.

The yield function of the isochoric expansive growth is discussed first. Following Spencer's invariant theory (Spencer, 2001), two invariants of Spencer's deviatoric stress tensor can be defined as

$$\bar{J}_1(\overline{\boldsymbol{S}}^{DEV}, \overline{\boldsymbol{a}}/\sqrt{\lambda_{\boldsymbol{a}}}) = \frac{1}{\lambda_{\boldsymbol{a}}}\|\overline{\boldsymbol{S}}^{DEV}\overline{\boldsymbol{C}}\overline{\boldsymbol{S}}^{DEV}\|_{\overline{\boldsymbol{a}}} \equiv (\boldsymbol{\tau}^{dev}\tilde{\boldsymbol{a}})\cdot(\boldsymbol{\tau}^{dev}\tilde{\boldsymbol{a}}) = \tilde{J}_1(\boldsymbol{\tau}^{dev}, \tilde{\boldsymbol{a}}) \tag{42}$$

and

$$\bar{J}_2(\overline{\boldsymbol{S}}^{DEV}) = \mathrm{Tr}(\overline{\boldsymbol{S}}^{DEV}\overline{\boldsymbol{C}}\overline{\boldsymbol{S}}^{DEV}) \equiv \boldsymbol{\tau}^{dev} : \boldsymbol{\tau}^{dev} = \tilde{J}_2(\boldsymbol{\tau}^{dev}). \tag{43}$$

The invariant $\bar{J}_1$ (or $\tilde{J}_1$) is a fibre-dependent invariant. On the other hand, $\bar{J}_2$(or $\tilde{J}_2$) is the natural counterpart of $J_2(=\frac{1}{2}\mathrm{dev}[\boldsymbol{\tau}] : \mathrm{dev}[\boldsymbol{\tau}])$ in the classical J_2-viscoplasticity theory. Based on this observation, a natural generalization of the yield function for isochoric expansive growth which is consistent with the classical von Mises yield condition is written as

$$f_{dev}(\overline{\boldsymbol{S}}^{DEV}, \overline{\boldsymbol{a}}/\sqrt{\lambda_{\boldsymbol{a}}}, \alpha) = \frac{\bar{J}_1}{Y_1^2} + \frac{\bar{J}_2}{Y_2^2} - (1 + h(\alpha)) \equiv \frac{\tilde{J}_1}{Y_1^2} + \frac{\tilde{J}_2}{Y_2^2} - (1 + h(\alpha)) = \tilde{f}_{dev}(\boldsymbol{\tau}^{dev}, \tilde{\boldsymbol{a}}, \alpha) \tag{44}$$

where Y_1 and Y_2 are two yield parameters with dimensions of stress, h is a scalar hardening function in terms of the hardening parameter α. A hardening potential is assumed as $H = \frac{1}{2}K\alpha^2$. Then a stress-like variable, q, is defined as

$$q = \frac{\partial H}{\partial \alpha} = K\alpha. \tag{45}$$

The yield function of volumetric growth, f_{vol}, is suggested in the same format as that of J_2-viscoplasticity as

$$f_{vol}(\overline{\boldsymbol{S}}^A) = \bar{I}_2(\overline{\boldsymbol{S}}^A) - (Y_3 + h_{vol}(\alpha, \alpha_{vol})) \equiv I_2(\boldsymbol{\tau}^A) - (Y_3 + h_{vol}(\alpha, \alpha_{vol})) = \tilde{f}_{vol}(\boldsymbol{\tau}^A) \tag{46}$$

where the second invariant $\bar{I}_2$ (or I_2) is defined as

$$\bar{I}_2(\bar{\boldsymbol{S}}^A)=\tfrac{1}{2}\left((\mathrm{Tr}\bar{\boldsymbol{S}}^A)^2-\mathrm{Tr}(\bar{\boldsymbol{S}}^A\bar{\boldsymbol{C}}\bar{\boldsymbol{S}}^A)\right)\equiv\tfrac{1}{2}((\mathrm{tr}\boldsymbol{\tau}^A)^2-\boldsymbol{\tau}^A:\boldsymbol{\tau}^A)=I_2(\boldsymbol{\tau}^A) \tag{47}$$

where Y_3 is the yield threshold and h_{vol} is a scalar hardening function in terms of hardening parameters α and α_{vol}. It is noted that h_{vol} represents the coupling between α and α_{vol}. Similar to Eq. (45), the corresponding stress-like variable, q_{vol}, is defined as

$$q_{vol}=K_{vol}\alpha_{vol} \tag{48}$$

where K_{vol} is the isotropic hardening modulus.

Similarly, the yield function of microfibrils extension, f_{λ_a}, is defined in the same format as that of J_2-viscoplasticity as

$$f_{\lambda_a}(\bar{\boldsymbol{S}})=\bar{\tau}_{\lambda_a}(\bar{\boldsymbol{S}})-(Y_4+h_{\lambda_a}(\alpha,\alpha_{\lambda_a}))\equiv\tau_{\lambda_a}(\boldsymbol{\tau})-(Y_4+h_{\lambda_a}(\alpha,\alpha_{\lambda_a}))=\tilde{f}_{\lambda_a}(\boldsymbol{\tau}) \tag{49}$$

where Y_4 is yield threshold and h_{λ_a} is scalar hardening function in terms of hardening parameters α and α_{λ_a}. Again, a stress-like variables, q_{λ_a}, is defined as

$$q_{\lambda_a}=K_{\lambda_a}\alpha_{\lambda_a} \tag{50}$$

where K_{λ_a} is the isotropic hardening modulus.

4.3. Overstress functions

In his fibre-reinforced viscoplastic model, Spencer (2001) proposed a flow rule of the Duvaut–Lions type (Simo and Hughes, 1998) which needs to calculate the closest point projection of Spencer's deviatoric stress onto the yield surface. Such a model involves nonlinear equations for solving the closest point projection in the space of the stress *tensor* that can lead to considerable extra computation. In the present study, a flow rule using the Perzyna model (Simo and Hughes, 1998) is suggested which involves the overstress function defined in the space of invariants of stress. Corresponding to the decomposition of growth, there are a set of three overstress functions for the driving forces proposed in the preceding discussion.

First we discuss the overstress function for the isochoric expansive growth. It is noted that in classic viscoplasticity, the overstress function of the Perzyna model was defined as a function of yield function since yield function has the same dimension of stress (Simo and Hughes, 1998). However, the yield function in Eq. (44) is dimensionless. In order to obtain the overstress function for isochoric expansive growth in terms of Spencer's deviatoric stress tensor $\bar{\boldsymbol{S}}^{DEV}$, a naturally generalized overstress function is defined in terms of the minimum distance between the current stress point, which is outside the yield surface, and the yield surface in the space of invariants, $\mathcal{S}_{\bar{J}}=\{\sqrt{\bar{J}_1},\sqrt{\bar{J}_2}\}\subseteq R^+\times R^+$, in which R^+ denotes the set of non-negative real numbers. The consistence of this generalization with the Perzyna model can be justified by the fact that in J_2-viscoplasticity an overstress function is the minimum distance between the point $\sqrt{J_2}$ and the yield surface.

As shown in Fig. 4, given a point $\bar{\boldsymbol{J}}=(\sqrt{\bar{J}_1},\sqrt{\bar{J}_2})\in\mathcal{S}_{\bar{J}}$, a measure function between this point and any other point $\tilde{\boldsymbol{\theta}}=(\tilde{\theta}_1,\tilde{\theta}_2)\in\mathcal{S}_{\bar{J}}$ is defined as

$$\tilde{\phi}(\tilde{\boldsymbol{\theta}}\bar{\boldsymbol{J}})=\sqrt{(\bar{\boldsymbol{J}}-\tilde{\boldsymbol{\theta}})\cdot(\bar{\boldsymbol{J}}-\tilde{\boldsymbol{\theta}})}\quad\forall\tilde{\boldsymbol{\theta}}\in\mathcal{S}_{\bar{J}}. \tag{51}$$

Then a distance function, $\phi(\bar{\boldsymbol{\theta}}\bar{\boldsymbol{J}})$, representing the minimum distance between the given point $\bar{\boldsymbol{J}}$ and the yield surface $f_{dev}=0$ can be defined as

$$\left.\begin{aligned}&\phi(\bar{\boldsymbol{\theta}}\bar{\boldsymbol{J}})=\min_{\tilde{\boldsymbol{\theta}}\in\mathcal{S}_{\bar{J}}}\tilde{\phi}(\tilde{\boldsymbol{\theta}}\bar{\boldsymbol{J}})\\&s.t.\ f_{dev}(\tilde{\boldsymbol{\theta}},\alpha)=\tfrac{\tilde{\theta}_1^2}{Y_1^2}+\tfrac{\tilde{\theta}_2^2}{Y_2^2}-(1+h(\alpha))=0\end{aligned}\right\} \tag{52}$$

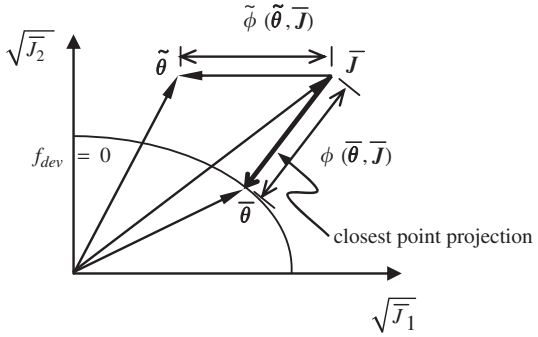

Fig. 4. Closest point projection in the space of stress invariants.

where *s.t.* denotes 'subject to (the constraint)'. The point $\overline{\boldsymbol{\theta}}$ is the closest point projection of $\overline{\boldsymbol{J}}$ onto the yield surface.

For solving the constrained minimum problem in Eq. (52), an equivalent unconstrained formulation is written as

$$\phi(\overline{\boldsymbol{\theta}}\overline{\boldsymbol{J}}) = \min_{\tilde{\boldsymbol{\theta}}\in\mathcal{S}_j}\{\tilde{\phi}(\tilde{\boldsymbol{\theta}}\overline{\boldsymbol{J}}) - \theta f_{dev}(\tilde{\boldsymbol{\theta}},\alpha)\} \tag{53}$$

by introducing a Lagrangian multiplier, θ. By solving Eq. (53), the closest point $\overline{\boldsymbol{\theta}}$ is obtained as

$$\overline{\boldsymbol{\theta}} = \left\{ \begin{array}{c} \sqrt{\overline{J}_1}/(1-\theta/Y_1^2) \\ \sqrt{\overline{J}_2}/(1-\theta/Y_2^2) \end{array} \right\}, \tag{54}$$

and the distance function is

$$\phi(\overline{\boldsymbol{\theta}}\overline{\boldsymbol{J}}) = -\theta\sqrt{\frac{\overline{J}_1}{(Y_1^2-\theta)^2} + \frac{\overline{J}_2}{(Y_2^2-\theta)^2}} \tag{55}$$

where the Lagrange multiplier θ is one of the real roots of a quartic equation

$$(1+h)(\theta-Y_1^2)^2(\theta-Y_2^2)^2 - \overline{J}_2 Y_2^2(\theta-Y_1^2)^2 - \overline{J}_1 Y_1^2(\theta-Y_2^2)^2 = 0 \tag{56}$$

which by comparison with other real roots, gives the smallest non-negative ϕ.

With the distance function ϕ calculated, the overstress function for isochoric expansive growth can be defined as

$$\overline{\phi}_{dev} = \left\{ \begin{array}{ll} 0 & \text{if } f_{dev}(\overline{\boldsymbol{S}}^{DEV}, \overline{\boldsymbol{a}}/\sqrt{\lambda_{\boldsymbol{a}}}, \alpha) \le 0 \\ \phi^m & \text{if } f_{dev}(\overline{\boldsymbol{S}}^{DEV}, \overline{\boldsymbol{a}}/\sqrt{\lambda_{\boldsymbol{a}}}, \alpha) > 0 \end{array} \right. \tag{57}$$

where m is a rate-sensitivity exponent.

The overstress function $\overline{\phi}_{dev}$ is *implicitly* defined as a function of yield function f_{dev}. By contrast, following the classical J_2-viscoplasticity theory, the overstress functions for volumetric growth and irreversible microfibrils extension are defined explicitly as the functions of the corresponding yield functions as

$$\overline{\phi}_{vol} = \langle f_{vol} \rangle/2, \quad \overline{\phi}_{\lambda_{\boldsymbol{a}}} = \langle f_{\lambda_{\boldsymbol{a}}} \rangle/2, \tag{58}$$

respectively, where $\langle \cdot \rangle$ denotes a ramp function, $\langle x \rangle = (x+|x|)/2$.

4.4. Flow rule

The expansive growth of cell wall generally is dominated by the elongation in a particular direction. Based on this fact, by adopting the assumption that the plastic spin, $\mathrm{skw}\overline{\boldsymbol{L}}^g$, vanishes, it is sufficient to specify the flow rule as the evolution of $\overline{\boldsymbol{D}}^g$.

Following the penalty formulation proposed by Simo and Hughes (1998), the principle of maximum dissipation is represented as an unconstrained minimization problem as follows:

$$\begin{aligned} &\min_{(\overline{\boldsymbol{S}},\overline{\boldsymbol{q}})\in\mathcal{S}\times\mathbb{R}^3}\left\{-D_\eta(\overline{\boldsymbol{S}},\overline{\boldsymbol{q}},\overline{\boldsymbol{D}}^g,\dot{\overline{\boldsymbol{\alpha}}})\right\} \\ &D_\eta(\overline{\boldsymbol{S}},\overline{\boldsymbol{q}},\overline{\boldsymbol{D}}^g,\dot{\overline{\boldsymbol{\alpha}}}) = \overline{\boldsymbol{S}} : \overline{\boldsymbol{D}}^g + \overline{\boldsymbol{q}}\cdot\dot{\overline{\boldsymbol{\alpha}}} - \frac{1}{\eta}(\gamma^+(\overline{\phi}_{dev}) + \beta_1\gamma^+(\overline{\phi}_{vol}) + \beta_2\gamma^+(\overline{\phi}_{\lambda_{\boldsymbol{a}}})) \end{aligned} \tag{59}$$

where $\overline{\boldsymbol{\alpha}} = \left\{ \begin{array}{ccc} \alpha & \alpha_{vol} & \alpha_{\lambda_{\boldsymbol{a}}} \end{array} \right\}^T$ and $\overline{\boldsymbol{q}} = \left\{ \begin{array}{ccc} q & q_{vol} & q_{\lambda_{\boldsymbol{a}}} \end{array} \right\}^T$, $\mathcal{S}$ denotes the vector space of symmetric second order tensors, β_1 and β_2 are two weighted parameters, η is so-called penalty function, and the function $\gamma^+(\cdot)$ is defined as (Simo and Hughes, 1998)

$$\gamma^+(x) = \left\{ \begin{array}{ll} \frac{1}{2}x^2 & \text{if } x \ge 0 \\ 0 & \text{if } x < 0 \end{array} \right. . \tag{60}$$

Solving the minimization problem in Eq. (59) yields two optimality conditions

$$-\frac{\partial D_\eta}{\partial \overline{\boldsymbol{S}}} = 0, \quad -\frac{\partial D_\eta}{\partial \overline{\boldsymbol{q}}} = 0. \tag{61}$$

The first optimality condition $-\partial D_\eta/\partial\overline{\boldsymbol{S}} = 0$ yields a general format of growth flow rule on $\overline{\mathcal{B}}_t$ in the following form:

$$\overline{\boldsymbol{D}}^g = \dot{\lambda}\frac{\partial\overline{\phi}_{dev}}{\partial\overline{\boldsymbol{S}}} + \dot{\lambda}_{vol}\frac{\partial\overline{\phi}_{vol}}{\partial\overline{\boldsymbol{S}}} + \dot{\lambda}_{\lambda_{\boldsymbol{a}}}\frac{\partial\overline{\phi}_{\lambda_{\boldsymbol{a}}}}{\partial\overline{\boldsymbol{S}}} \tag{62}$$

where the rates of effective viscoplastic strains are formulated as

$$\dot{\lambda} = \frac{\overline{\phi}_{dev}}{\eta}, \quad \dot{\lambda}_{vol} = \frac{\overline{\phi}_{vol}}{\eta/\beta_1}, \quad \dot{\lambda}_{\lambda_{\boldsymbol{a}}} = \frac{\overline{\phi}_{\lambda_{\boldsymbol{a}}}}{\eta/\beta_2}. \tag{63}$$

The penalty function η is recognised as a temperature-dependent viscosity which is defined in a format of the Arrhenius equation

$$\eta = \eta_0 \exp(-Q/R(T-T_0)) \tag{64}$$

where η_0, T_0 and activation energy Q are three parameters obtained by fitting experimental data and $R(=8.314472\ \mathrm{J/K\ mol})$ is the gas constant. Functions η/β_1 and η/β_2 are the matrix bulk viscosity and the microfibrils uniaxial viscosity, respectively.

To obtain the expression of the tensor $\partial\overline{\phi}_{dev}/\partial\overline{\boldsymbol{S}}$ in Eq. (62), the derivative $\partial\overline{\phi}_{dev}/\partial\boldsymbol{\tau}$ is calculated and then mapped back from $\mathcal{B}_t$ onto $\overline{\mathcal{B}}_t$ with the relationship (Belytschko et al., 2001)

$$\frac{\partial(\cdot)}{\partial\overline{\boldsymbol{S}}} = \boldsymbol{F}^{eT}\frac{\partial(\cdot)}{\partial\boldsymbol{\tau}}\boldsymbol{F}^{e}. \tag{65}$$

As $\overline{\phi}_{dev}$(such that $\overline{\phi}_{dev}\neq 0$) is the function in terms of $\bar{J}_1$ and $\bar{J}_2$ (or $\tilde{J}_1$ and $\tilde{J}_2$ equivalently), by using Eq. (A4) in Appendix A and the chain rule, a viscoplastic flow tensor sym$\boldsymbol{R}^*$ is obtained as

$$\mathrm{sym}\boldsymbol{R}^* = \frac{\partial\overline{\phi}_{dev}}{\partial\boldsymbol{\tau}} = \beta_3\frac{\partial\tilde{J}_1}{\partial\boldsymbol{\tau}} + \beta_4\frac{\partial\tilde{J}_2}{\partial\boldsymbol{\tau}} \tag{66}$$

where two functions, β_3 and β_4, are defined as

$$\beta_3 = m\phi^{m-1}\left(\frac{\partial\phi}{\partial\bar{J}_1} + \vartheta_1\frac{\partial\phi}{\partial\theta}\right), \quad \beta_4 = m\phi^{m-1}\left(\frac{\partial\phi}{\partial\bar{J}_2} + \vartheta_2\frac{\partial\phi}{\partial\theta}\right). \tag{67}$$

By taking the derivative of Eqs. (42) and (43), the expressions of $\partial\tilde{J}_1/\partial\boldsymbol{\tau}$ and $\partial\tilde{J}_2/\partial\boldsymbol{\tau}$ are obtained as follows:

$$\frac{\partial\tilde{J}_1}{\partial\boldsymbol{\tau}} = \tilde{\boldsymbol{A}}\boldsymbol{\tau}^{dev} + \boldsymbol{\tau}^{dev}\tilde{\boldsymbol{A}}, \quad \frac{\partial\tilde{J}_2}{\partial\boldsymbol{\tau}} = 2\boldsymbol{\tau}^{dev}. \tag{68}$$

In a similar manner to Eq. (40), it can be proved straightforwardly that

$$(\tilde{\boldsymbol{A}}\boldsymbol{\tau}^{dev} + \boldsymbol{\tau}^{dev}\tilde{\boldsymbol{A}}) : \boldsymbol{A} = 0, \quad \mathrm{tr}(\tilde{\boldsymbol{A}}\boldsymbol{\tau}^{dev} + \boldsymbol{\tau}^{dev}\tilde{\boldsymbol{A}}) = 0. \tag{69}$$

Eqs. (40) and (69) indicate that the tensor sym$\boldsymbol{R}^*$, which is defined in Eq. (66) as a linear combination of $\partial\tilde{J}_1/\partial\boldsymbol{\tau}$ and $\partial\tilde{J}_2/\partial\boldsymbol{\tau}$, satisfies the kinematic conditions of an isochoric viscoplastic flow without plastic extension in the direction of microfibrils, i.e. sym$\boldsymbol{R}^*$:$\boldsymbol{A}$=0 and tr(sym$\boldsymbol{R}^*$)=0. By substituting Eq. (66) into Eq. (65), the plastic flow direction of part I of the growth on $\overline{\mathcal{B}}_t$ is obtained as

$$\mathrm{sym}\overline{\boldsymbol{R}}^* = \frac{\partial\overline{\phi}_{dev}}{\partial\overline{\boldsymbol{S}}} = \beta_3\left[\hat{\boldsymbol{A}}\overline{\boldsymbol{\Sigma}}^{DEV} + (\hat{\boldsymbol{A}}\overline{\boldsymbol{\Sigma}}^{DEV})^T\right] + 4\beta_4\mathrm{sym}\overline{\boldsymbol{\Sigma}}^{DEV} \tag{70}$$

where $\overline{\boldsymbol{\Sigma}}^{DEV}$ is a form of the Mandel stress (Mandel, 1971; Lubliner, 1990)

$$\overline{\boldsymbol{\Sigma}}^{DEV} = \overline{\boldsymbol{S}}^{DEV}\overline{\boldsymbol{C}}. \tag{71}$$

Mandel stress is a degenerate form of the Eshelby (energy-momentum) tensor which has been hypothesised to be the driving force of growth (Imatani and Maugin, 2002).

The plastic flow direction of volumetric growth is defined on $\mathcal{B}_t$ as

$$\boldsymbol{R}^*_{vol} = \frac{\partial\overline{\phi}_{vol}}{\partial\boldsymbol{\tau}} = \left\{\mathrm{tr}\boldsymbol{\tau}^A\right\}\boldsymbol{R}_{vol} - \boldsymbol{\tau}^A \tag{72}$$

where the tensor $\boldsymbol{R}_{vol}$ is defined as

$$\boldsymbol{R}_{vol} = \boldsymbol{1} - \tilde{\boldsymbol{A}} \tag{73}$$

which satisfies the condition $\boldsymbol{R}_{vol}$:$\boldsymbol{A}$=0. Tensor $\boldsymbol{R}_{vol}$ is the unit tensor in the plane perpendicular to the direction of microfibrils, $\tilde{\boldsymbol{a}}$. By using Eq. (65), the equivalent flow direction on $\overline{\mathcal{B}}_t$ is obtained as

$$\overline{\boldsymbol{R}}^*_{vol} = \frac{\partial\overline{\phi}_{vol}}{\partial\overline{\boldsymbol{S}}} = \left\{\mathrm{Tr}\overline{\boldsymbol{S}}^A\right\}\overline{\boldsymbol{R}}_{vol} - \overline{\boldsymbol{C}}\overline{\boldsymbol{S}}^A\overline{\boldsymbol{C}} \tag{74}$$

where tensor $\overline{\boldsymbol{R}}_{vol}$ is defined by pulling back $\boldsymbol{R}_{vol}$ from $\mathcal{B}_t$ onto $\overline{\mathcal{B}}_t$ as

$$\overline{\boldsymbol{R}}_{vol} = \overline{\boldsymbol{C}} - \hat{\boldsymbol{A}}. \tag{75}$$

Tensor $\boldsymbol{R}^*_{vol}$ satisfies the condition $\boldsymbol{R}^*_{vol} : \boldsymbol{A} = 0$, so it is an admissible flow direction of part II of the growth. Tensor $\boldsymbol{R}^*_{vol}$ has clear geometric and physical meanings. To explain the geometric meaning of $\boldsymbol{R}^*_{vol}$, Eq. (72) is rearranged as $\boldsymbol{R}^*_{vol} + \boldsymbol{\tau}^A = \{\mathrm{tr}\boldsymbol{\tau}^A\}\boldsymbol{R}_{vol}$. Thus $\boldsymbol{R}^*_{vol}$ and $\boldsymbol{\tau}^A$ are the complementary parts of an additive decomposition of the 'unit' tensor $\boldsymbol{R}_{vol}$. Tensor $\boldsymbol{R}^*_{vol}$ yields a flow direction which compensates the wall-thinning resulting from the stress $\boldsymbol{\tau}^A$. On the other hand, tensor $\overline{\boldsymbol{R}}^*_{vol}$ is consistent with the first order volumetric growth model suggested by Epstein and Maugin (1996, 2000). By using the novel concept of material force, Epstein and Maugin came to the conclusion that the transplant (growth) tensor

of volumetric growth is a function in terms of the static Eshelby stress tensor, $\{\Psi\}\overline{\boldsymbol{C}}-\overline{\boldsymbol{CSC}}$, which by comparison with Eq. (74) is consistent with $\overline{\boldsymbol{R}}^{*}_{vol}$.

By using Eqs. (30), (49), (58) and the chain rule, tensor $\partial\overline{\phi}_{\lambda_a}/\partial\overline{\boldsymbol{S}}$, which represents the plastic flow direction of part III of the growth, is obtained as

$$\frac{\partial\overline{\phi}_{\lambda_a}}{\partial\overline{\boldsymbol{S}}}=\overline{\boldsymbol{R}}_{\lambda_a}. \tag{76}$$

Substituting Eqs. (70), (74), and (76) into the right side of Eq. (62), we obtain a flow rule of cell wall growth as

$$\overline{\boldsymbol{D}}^{g}=\dot{\lambda}\,\mathrm{sym}\overline{\boldsymbol{R}}^{*}+\dot{\lambda}_{vol}\overline{\boldsymbol{R}}^{*}_{vol}+\dot{\lambda}_{\lambda_a}\overline{\boldsymbol{R}}_{\lambda_a}. \tag{77}$$

It is noted that the structure of Eq. (77) is somewhat similar to that of the so-called evolution of transplant tensor proposed by Maugin and co-workers (Epstein and Maugin, 1996, 2000; Imatani and Maugin, 2002) although there are many differences between their contents. This structural similarity may not be a coincidence and indicates one of the general characteristics of growth.

From the point of view of biology, it is worth mentioning that the local plastic flow, $\overline{\boldsymbol{D}}^{g}$, plays the role of regulating the global growth of cell wall in a particular direction. Plant cells rarely enlarge isotropically; instead, they grow preferentially in a single direction (Marga et al., 2005). In order to account for this anisotropic growth under uniform turgor pressure, the prevalent existing elastic models assumed that cellulose microfibrils have a much larger Young's modulus than that of the cell wall matrix. This assumption, although succeeding to a certain extent in representing anisotropic growth, imposes a strong but somewhat loosely defined constraint on the elastic properties of the cell wall rather than on the irreversible growth. This is neither consistent with the well-accepted hypothesis that cell wall growth is regulated by biological mechanisms such as wall yielding (Cosgrove, 1993b; Schopfer, 2006; Verbelen and Vissenberg, 2007) nor with the observation that the alignment of microfibrils is insufficient to control growth anisotropy (Baskin, 2005). Therefore, being consistent with the biological mechanisms and taking advantage of the multiplicative decomposition in Eq. (6), the plastic flow rule defined by Eq. (77) is used to achieve the anisotropic growth in the present model. No elastic modulus constraint is required.

Hitherto, the three parts of the cell wall growth are modelled independently to clarify their growth mechanisms. Part III of the growth is negligible in *in vivo* cell wall growth (Marga et al., 2005). Therefore, the integrative model in this study is restricted to the cell wall growth without a plastic extension of microfibrils. In order to obtain such an integrative growth model, the interplays between the parts I and II of the growth are discussed at both molecular level and macroscopic level. The former leads to the hardening law, and the latter to the control equation of wall thickness.

4.5. Interplay between isochoric expansion and volumetric growth (1): hardening law

The second optimality condition, $-\partial D_{\eta}/\partial\overline{\boldsymbol{q}}=0$, in Eq. (61) together with Eqs. (45), (48), (50), (63) and the chain rule yield the following hardening law:

$$\dot{\alpha}=\frac{1}{K}\left(\frac{\partial\overline{\phi}_{dev}}{\partial\alpha}\dot{\lambda}+\frac{\partial\overline{\phi}_{vol}}{\partial\alpha}\dot{\lambda}_{vol}+\frac{\partial\overline{\phi}_{\lambda_a}}{\partial\alpha}\dot{\lambda}_{\lambda_a}\right),\quad \dot{\alpha}_{vol}=\frac{1}{K_{vol}}\frac{\partial\overline{\phi}_{vol}}{\partial\alpha_{vol}}\dot{\lambda}_{vol},\quad \dot{\alpha}_{\lambda_a}=\frac{1}{K_{\lambda_a}}\frac{\partial\overline{\phi}_{\lambda_a}}{\partial\alpha_{\lambda_a}}\dot{\lambda}_{\lambda_a}, \tag{78}$$

in which the function $\partial\overline{\phi}_{dev}/\partial\alpha$ ($\overline{\phi}_{dev}\neq 0$) is calculated by using Eqs. (57) and (A4) as

$$\frac{\partial\overline{\phi}_{dev}}{\partial\alpha}=m\overline{\phi}^{m-1}\vartheta_h\frac{\partial\overline{\phi}}{\partial\theta}\frac{\partial h}{\partial\alpha}, \tag{79}$$

while the other two functions, $\partial\overline{\phi}_{vol}/\partial\alpha_{vol}$and $\partial\overline{\phi}_{\lambda_a}/\partial\alpha_{\lambda_a}$, are straightforward derivatives.

The evolution of hardening parameters in Eq. (78) depends on the specified hardening functions $h(\alpha)$, $h_{vol}(\alpha,\alpha_{vol})$ and $h_{\lambda_a}(\alpha,\alpha_{\lambda_a})$. However, instead of constructing these functions, a direct mechanism-based method is suggested to obtain the evolution equation of α consistent with Eq. (78).

4.5.1. Mechanism-based hardening law

As aforementioned in the mechanism of part I of the growth, the isochoric expansive growth is the direct result of the enzymatic yielding passively driven by the stress. As the cell wall expands, additional cross-links come under load. As the number of load-bearing cross-links increases, the wall stiffens. This wall-hardening directly driven by the stress is an intrinsic property of the cell wall since it was observed in both the isolated walls and the living cells (Proseus and Boyer, 2006). Thus the irreversible change of the number of load-bearing cross-links is taken as the sole mechanism of hardening in the present model.

For the isolated wall there is no other mechanism to counter the hardening mechanism so that expansive growth decelerates and then stops inevitably. By contrast, new material deposition, which is usually considered as a process maintaining the strength of the wall, also plays the role of countering the hardening to create a growth-sustaining activity at molecular scale by the molecular assembly in the living cell (Proseus and Boyer, 2007).

To obtain a well-defined hardening law, two assumptions are used here. One is the assumption of length preservation of a cross-link which states that a cross-link can change its deformed state (i.e. conformation (Treloar, 2005)) or be

broken/reconnected but its total length is fixed when it is mapped from the reference configuration onto the intermediate configurations. The other is the topology preservation assumption which states that during the growth a broken cross-link can only reconnect into the load-bearing network in a manner to recover its original connectivity. In other words, the broken bonds of a cross-link are not allowed to connect with the bonds of the other cross-links (see Fig. 5(a)).

With the topology preservation assumption, a cross-link always keeps its identity (label) unaffected by the breaking or reconnection during growth. Thus the number of cross-links in a representative element is not changed by the breaking or

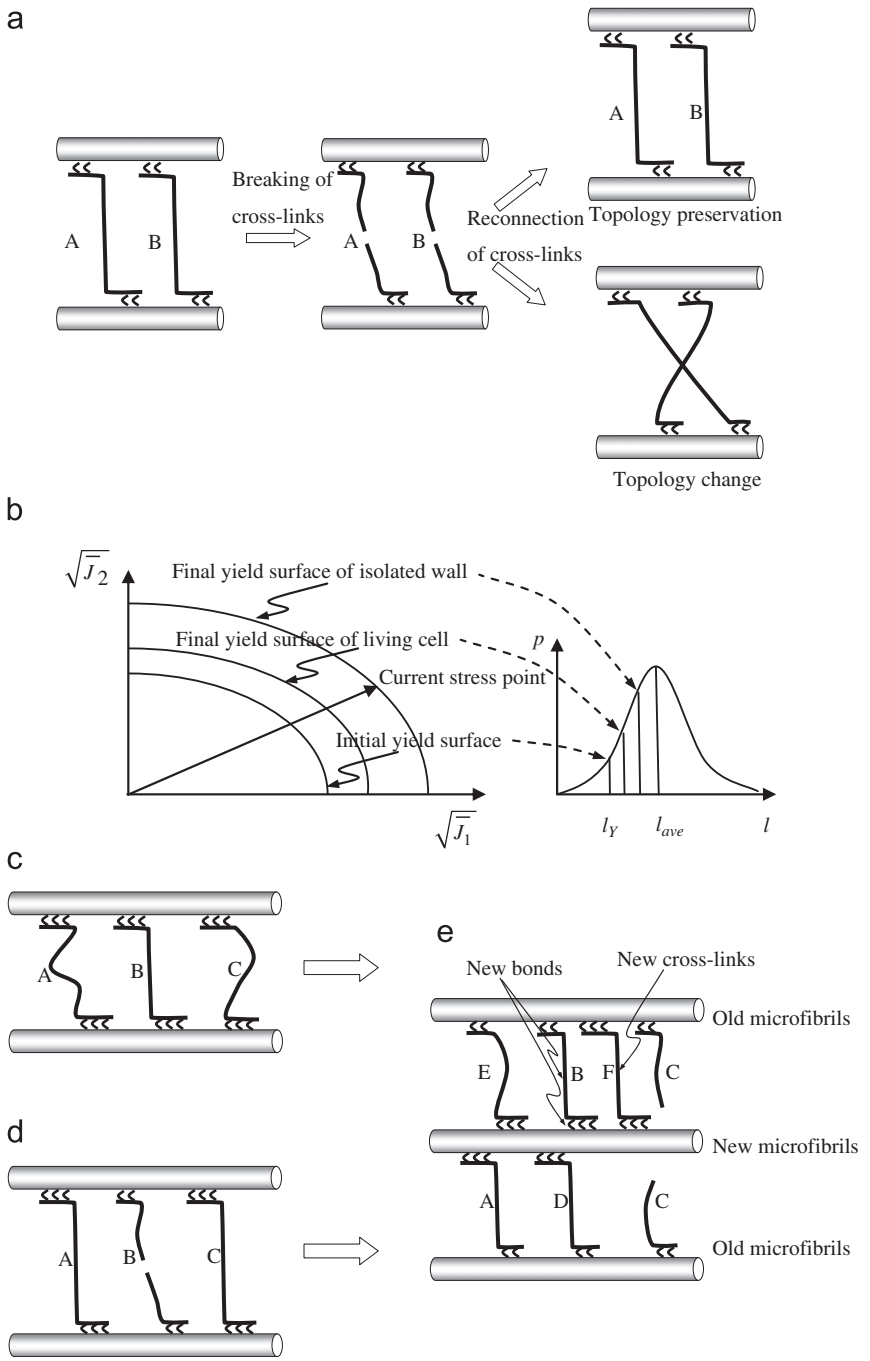

Fig. 5. Mechanism of hardening law and the change of load-bearing cross-links. (a) Topology preservation of cross-links and (b) schematic relationship between the evolution of yield surface and the probability density of load-bearing cross-links. (c) When cell wall starts to yield, shorter cross-link B sustain stress. (d) As growth continues, covalent bond and hydrogen bonds of cross-link B are broken and longer cross-links A and C start to sustain the stress. (e) As new material deposits, the new microfibrils and new cross-links D, E, F are inserted into and the broken cross-links A and B become load-bearing once again with new bonds generated to reconnect them into the load-bearing network.

reconnection if we count the labels (see Fig. 5(a), cross-links A and B). This makes the number of cross-links a well-defined quantity on $\overline{\mathcal{B}}_t$. Therefore, being consistent with the mechanism proposed by Proseus and Boyer (2007), we suggest that the hardening parameter α is taken as the *number fraction* of the load-bearing cross-links in a representative element on $\overline{\mathcal{B}}_t$ which is defined as the ratio of the number of the plastic load-bearing cross-links to the total number of the cross-links associated with growth.

We assume that the lengths of growth-associated cross-links, l, follow a certain probability distribution, $p(l)$, uniformly on the reference configuration. The present study is restricted to the cases in which either no new material is deposited (isolated wall) or the cross-links in new material have the same length distribution $p(l)$ as in the wall (living cell). Thus, according to the length and topology preservation assumptions, the length distribution $p(l)$ is preserved on $\overline{\mathcal{B}}_t$.

With hardening parameter α and length distribution $p(l)$ defined on $\overline{\mathcal{B}}_t$, the hardening law is established based on the connection between α and $p(l)$ as illustrated schematically in Fig. 5 where Gaussian distribution, $p(l)=\exp(-(l-l_{ave})^2/2b^2)/\sqrt{2\pi b^2}$ in which l_{ave} and b^2 are the average length and variance, respectively, is used. The mechanism of hardening is described as follows.

The interpretation of the yield threshold, Y, in the Lockhart Eq. (1) is that the load-bearing elements in the wall require a minimum elastic strain for wall yielding to occur (Cosgrove, 1986). Once the cell wall undergoes this minimum elastic strain, growth-associated cross-links with a corresponding length $l_Y(<l_{ave})$ start to sustain stress (see Fig. 5(c), cross-link B). Therefore, the number fraction α is equal to $p(l_Y)$ when the cell wall starts to yield. As the wall expansion continues, the current load-bearing cross-links are loosened by cutting the tethers and breaking the hydrogen bonds probably through enzymatic action (Proseus et al., 1999). Then, the longer cross-links with length $l\ (>l_Y)$ are replaced to sustain the stress (see Fig. 5(d)). This 'load-bearing – then breaking – then replacing' process continues during the expansive growth with the length l increasing continuously. Since wall rupture does not occur, it is reasonable to assume that the lengths of load-bearing cross-links are restricted to a range of $l_Y<l<l_{ave}$ which means that most of cross-links are intact at any instant. Under this assumption, $p(l)$ is a monotonically increasing function of l as shown in Fig. 5(b). In other words, the cell wall hardens monotonically during expansion. For the isolated walls, this intrinsic hardening mechanism solely controls the parameter $\alpha(=p(l))$ which does not stop increasing until the dynamic yield surface expands to reach the current stress point and the driving force for growth vanishes (see Fig. 5(b)).

For the living cell, the hardening is countered and balanced by the 'wall-loosening' supplied by new material deposition (volumetric growth). The new material not only brings in new load-bearing cross-links from outside but also triggers the reconnection of the cut tethers and broken hydrogen bonds inside (see Fig. 5(e)) (Proseus et al., 1999). The rate of change of the number faction of the plastic load-bearing cross-links is formulated on the intermediate configuration as

$$\frac{D}{Dt}\int_\Omega \alpha \mathrm{d}\Omega=\int_\Omega \dot{p}(l(\alpha))\mathrm{d}\Omega-\int_\Omega p(l_Y)\mathrm{tr}\overline{\boldsymbol{D}}^g\mathrm{d}\Omega-\int_\Omega \gamma\alpha\mathrm{tr}\overline{\boldsymbol{D}}^g\mathrm{d}\Omega \tag{80}$$

where $l(\cdot)(=p^{-1}(\cdot))$, which represents the average length of the plastic load-bearing cross-links, is the inverse function of the length distribution $p(l)$ $(l_Y<l<l_{ave})$, Ω is a domain on the intermediate configuration, and γ is a coefficient. The first term on the right-hand side of Eq. (80) represents the contribution of the intrinsic hardening during the wall expansion. The second term indicates the contribution of new incoming load-bearing cross-links with the length l_Y. The third term accounts for the reconnected load-bearing cross-links inside the cell wall which are triggered by the new material. According to the hypothesis of auto-propagation of the load-bearing and calcium-exchange suggested by Proseus and Boyer (2007), when new material becomes available, the plastic load-bearing cross-links are capable of releasing their calcium to the broken bonds to reconnect the cross-links. Thus it is assumed that the contribution of the reconnected cross-links is a bilinear function of the current α and rate of volumetric growth $\mathrm{tr}\overline{\boldsymbol{D}}^g$.

By using the relationship $\frac{D}{Dt}\int_\Omega(\cdot)\mathrm{d}\Omega=\int_\Omega\frac{D}{Dt}(\cdot)+(\cdot)\mathrm{tr}\overline{\boldsymbol{D}}^g\mathrm{d}\Omega$, the local format of Eq. (80) is obtained as

$$\frac{D\alpha}{Dt}=\dot{p}(l(\alpha))-((1+\gamma)\alpha+p(l_Y))\mathrm{tr}\overline{\boldsymbol{D}}^g. \tag{81}$$

In order to obtain an evolution equation of α in the similar format as Eq. (78), function $p(l)$ is approximated by using its Taylor expansion at l_Y as $p(l)\approx p(l_Y)+\partial p/\partial l|_{l=l_Y}(l-l_Y)$. Thus we have $\dot{p}(l(\alpha))\equiv\partial p/\partial l|_{l=l_Y}\partial l/\partial t$. Let $\overline{\boldsymbol{n}}_l$ denote the average direction of the load-bearing cross-links in a representative element on $\overline{\mathcal{B}}_t$. Then a relationship between the local growth rate $\partial l/\partial t$ and the macroscopic rate of growth $\overline{\boldsymbol{D}}^g$ is assumed as $\partial l/\partial t=\overline{\boldsymbol{n}}_l\cdot\overline{\boldsymbol{D}}^g\cdot\overline{\boldsymbol{n}}_l$. Therefore Eq. (81) can be approximated as

$$\frac{D\alpha}{Dt}=\partial p/\partial l|_{l=l_Y}\overline{\boldsymbol{n}}_l\cdot\overline{\boldsymbol{D}}^g\cdot\overline{\boldsymbol{n}}_l-((1+\gamma)\alpha+p(l_Y))\mathrm{tr}\overline{\boldsymbol{D}}^g. \tag{82}$$

Substituting the flow rule in Eq. (77) into Eq. (82) yields

$$\frac{D\alpha}{Dt}=p_\lambda\dot{\lambda}+\left\{p_{\lambda_{vol}}-((1+\gamma)\alpha+p(l_Y))\mathrm{tr}\overline{\boldsymbol{R}}^*_{vol}\right\}\dot{\lambda}_{vol}+p_{\lambda_{\lambda_a}}\dot{\lambda}_{\lambda_a} \tag{83}$$

in which

$$p_\lambda=\partial p/\partial l|_{l=l_Y}\overline{\boldsymbol{n}}_l\cdot\mathrm{sym}\overline{\boldsymbol{R}}^*\cdot\overline{\boldsymbol{n}}_l,\quad p_{\lambda_{vol}}=\partial p/\partial l|_{l=l_Y}\overline{\boldsymbol{n}}_l\cdot\overline{\boldsymbol{R}}^*_{vol}\cdot\overline{\boldsymbol{n}}_l,\quad p_{\lambda_{\lambda_a}}=\partial p/\partial l|_{l=l_Y}\overline{\boldsymbol{n}}_l\cdot\overline{\boldsymbol{R}}_{\lambda_a}\cdot\overline{\boldsymbol{n}}_l. \tag{84}$$

Eq. (83), which has a similar form to Eq. (78), is the mechanism-based hardening law of the hardening parameter α. It is noted that, given boundary conditions, the parameter α can be solved from Eq. (83) if α is taken as an internal degree of freedom (Maugin, 1999).

4.5.2. Phenomenological hardening law

Based on the mechanism-based hardening law in Eq. (83), the expression of phenomenological hardening law can be suggested without using Eq. (78). We restrict the analysis to the integrative model without the plastic extension of microfibrils. Thus $\dot{\lambda}_{\lambda_a}$ vanishes. Moreover, there is a linear relationship between $\dot{\lambda}_{vol}$ and $\dot{\lambda}$, say $\dot{\lambda}_{vol}=\zeta\dot{\lambda}$, as shown in Eq. (93) or (96) which is discussed in the next section. With the two conditions, Eq. (83) is rewritten as

$$\dot{\alpha}=(h_1+h_2\alpha)\dot{\lambda} \tag{85}$$

where $h_1(>0)$ and $h_2(=0$ for isolated walls and <0 for living cells) are

$$h_1=p_\lambda+(p_{\lambda_{vol}}-p(l_Y)\mathrm{tr}\boldsymbol{R}^*_{vol})\zeta,\quad h_2=-(1+\gamma)\zeta\mathrm{tr}\boldsymbol{R}^*_{vol}. \tag{86}$$

Due to the anisotropy of growth, $\overline{\boldsymbol{n}}_l\cdot\overline{\boldsymbol{R}}^*_{vol}\cdot\overline{\boldsymbol{n}}_l$ in Eq. (84) tends to zero. Thus h_1 of the isolated wall ($\zeta=0$) is larger than that of the corresponding living cell ($\zeta>0$).

Eq. (85) can be taken as the phenomenological hardening law with two parameters, h_1 and h_2, to be estimated by experimental data rather than Eq. (86). Accordingly the term $\nabla\alpha$ in the material time derivative in Eq. (85) is ignored since in the phenomenological model α is an internal variable rather than an internal degree of freedom with a governing equation depending on $\nabla\alpha$ (Maugin, 1999).

Function $h(\alpha)$ in the yield function in Eq. (44) is suggested to be $h=\alpha$ which is simple enough for verifying the suggested evolution equation of α.

4.5.3. Analysis of a uniaxial viscoplastic model

To obtain an insight into how the phenomenological hardening law, Eq. (85), couples with the flow rule to regulate the growth in an integrative model, we study a uniaxial viscoplastic model (a modified Lockhart model with hardening) defined by Eq. (85) and a flow rule $\dot{\lambda}=(\sigma-\sigma_Y(1+\alpha))/\eta$ in which σ and σ_Y are the uniaxial stress and static yield threshold, respectively. With the conditions $\sigma=const.\geq\sigma_Y$ and $\lambda|_{t=0}=\alpha|_{t=0}=0$, the analytical solution of α in this uniaxial model is

$$\alpha(\bar{t})=\frac{C_1(1-C_2\bar{t}_s)+(1+C_2\bar{t}_s)e^{-\bar{t}/\bar{t}_s}}{2C_3\bar{t}_s(C_1-e^{-\bar{t}/\bar{t}_s})} \tag{87}$$

where $\bar{t}(=t/\eta)$ is a normalised time, $\bar{t}_s$, which is a normalised characteristic time for the saturation of α, is defined as

$$\bar{t}_s=1/|h_1\sigma_Y+h_2(\sigma-\sigma_Y)|, \tag{88}$$

and C_1, C_2 and C_3 are

$$C_1=\frac{C_2\bar{t}_s+1}{C_2\bar{t}_s-1},\quad C_2=h_1\sigma_Y-h_2(\sigma-\sigma_Y),\quad C_3=h_2\sigma_Y. \tag{89}$$

To understand the qualitative aspect of the uniaxial model, a limit yield stress, σ_Y^∞, is defined as

$$\sigma_Y^\infty=\sigma_Y(1+\alpha|_{\bar{t}\to+\infty}). \tag{90}$$

Substituting Eq. (87) into Eq. (90), we have

$$\sigma_Y^\infty=\min\{\sigma,\sigma_Y(1+(h_1/|h_2|))\}. \tag{91}$$

Fig. 6 illustrates how σ_Y^∞ and $\bar{t}_s$ depend on parameters h_1 and h_2 in which $\sigma=0.5$ MPa and $\sigma_Y=0.3$ MPa correspond to the experimental data of turgor pressure and yield threshold, respectively. Fig. 6(a) shows that if $|h_2|/h_1\leq\sigma_Y/(\sigma-\sigma_Y)$, we have $\sigma_Y^\infty=\sigma$. The physical meaning of this conclusion is that for an isolated wall ($h_2=0$), the growth is vanishing when $\bar{t}$ is much larger than $\bar{t}_s$ since the dynamic yield stress $\sigma_Y(1+\alpha)$ is approaching the limit $\sigma_Y^\infty(=\sigma)$. This conclusion is robust because a perturbation $\delta h_2(\neq0)$ from the ideal state of $h_2=0$ does not alter the conclusion if $|\delta h_2|/h_1<\sigma_Y/(\sigma-\sigma_Y)$. On the other hand, given $|h_2|/h_1>\sigma_Y/(\sigma-\sigma_Y)$, a living cell ($h_2<0$) has $\sigma_Y<\sigma_Y^\infty<\sigma$ which means the cell wall grows under a steady driving force, $\sigma-\sigma_Y^\infty$, when $\bar{t}$ is much larger than $\bar{t}_s$. The larger the parameter $|h_2|$, the larger is the driving force. In order words, a stronger new wall material deposition is associated with a faster expansive growth.

The relationship between the characteristic time $\bar{t}_s$ and the parameters h_1 and h_2 is shown in Fig. 6(b). The $\bar{t}_s$ vs. $|h_2|/h_1$ curves show a partition of the ($\bar{t}_s$, $|h_2|/h_1$) space by the line $|h_2|/h_1=\sigma_Y/(\sigma-\sigma_Y)$, which indicates the separation of the isolated walls and the living cells with sustainable growth. Fig. 6(c) presents a 'map' (diagram) of the space of parameters h_1 and h_2 which indicates the partition of the space of (h_1, h_2) corresponding to the three different growth states. Domain 1 refers to unsustainable growth (including isolated walls), domains 2 and 3 refer to sustainable growth of living cell walls. $\bar{t}_s^{wall}=1/(h_1\sigma_Y)$ is the characteristic time of the isolated wall.

Fig. 6, although derived from a study of a uniaxial model, illustrates that the mechanism-based hardening law in Eq. (83) and the corresponding phenomenological hardening law in Eq. (85) can properly represent the hardening behaviour of cell wall and the interplay between wall-stiffening and wall-loosening.

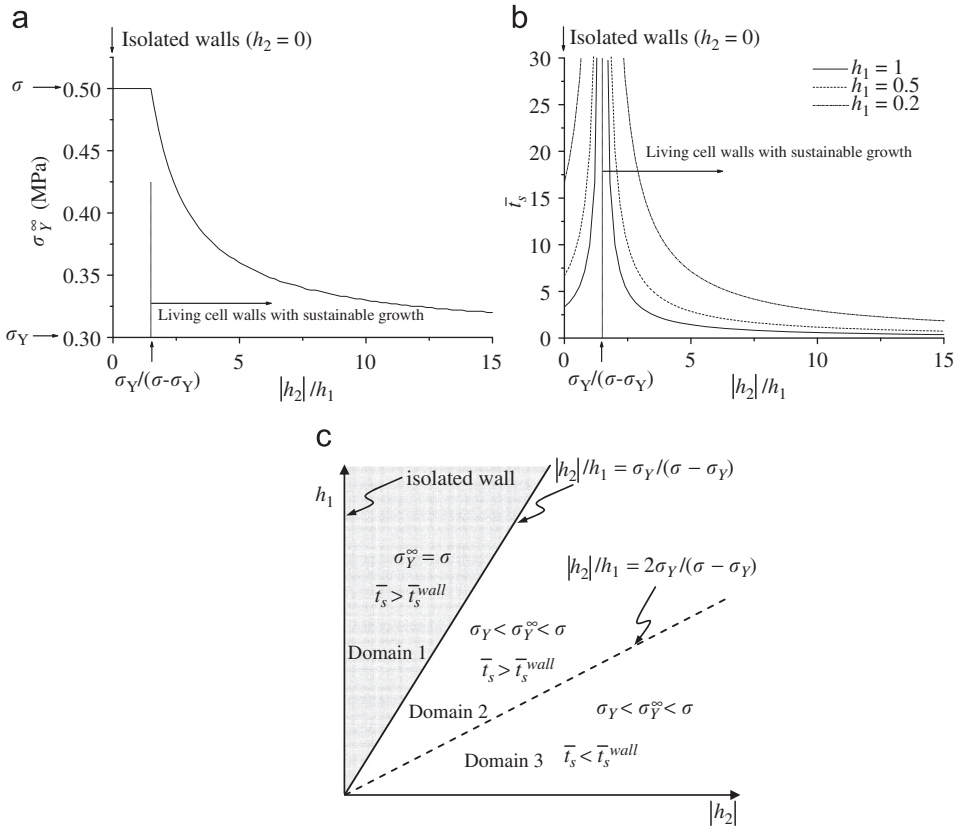

Fig. 6. Analysis of a uniaxial model (modified Lockhart model with hardening). (a) σ_Y^∞ vs. $|h_2|/h_1$ curve, (b) $\bar{t}_s$ vs. $|h_2|/h_1$ curves, and (c) partition of the h_1 and h_2 space.

4.6. *Interplay between isochoric expansion and volumetric growth (2): wall thickness*

Some researchers used the assumption of constant wall thickness as a geometric constraint to represent the interaction between the expansion and the new material deposition (Dumais et al., 2006; Dyson and Jensen, 2010). The assumption means that the rate of cell wall deposition is assumed to exactly match the rate of wall thinning due to stress-driven expansion. However, experimental observation reported that the wall may become thinner or thicker perhaps by as much as two-fold (Taiz, 1984; Kutschera, 1990). Moreover, the experiment of *in vitro* artificial expansive growth driven by rapid turgor pressure pulses (*P*-pulses) provided a case which did not agree with the constant wall thickness assumption (Proseus et al., 1999). In the experiment, the *P*-pulses were short enough to keep natural growth negligible. However, obvious irreversible expansion was observed, which can be considered as *in vitro* artificial growth. Therefore, it was clear that the assumption of constant wall thickness was violated since the wall deposition did not match the wall thinning during the *P*-pulses. In order to model this experimental observation, the assumption of constant wall thickness is replaced by a relaxed assumption that the cell wall can dynamically stabilise its thickness.

The condition of constant wall thickness imposes a constraint on the plastic flow rule on the current configuration $\mathcal{B}_t$ as

$$\boldsymbol{n}\cdot\boldsymbol{D}^g\cdot\boldsymbol{n}=0 \tag{92}$$

where vector $\boldsymbol{n}$ is the principal direction associated the minimum principal stress which roughly aligns with the unit normal vector perpendicular to the current cell wall surface. By using the flow rule in Eq. (77) and the fact that vector $\boldsymbol{n}$ is perpendicular to the direction of the microfibrils, i.e. $\boldsymbol{n}\cdot\boldsymbol{a}=0$, Eq. (92) yields

$$\dot{\lambda}_{vol}=\zeta\dot{\lambda},\quad \zeta=\frac{-\overline{\boldsymbol{n}}\cdot\mathrm{sym}\overline{\boldsymbol{R}}^*\cdot\overline{\boldsymbol{n}}}{\overline{\boldsymbol{n}}\cdot\overline{\boldsymbol{R}}^*_{vol}\cdot\overline{\boldsymbol{n}}} \tag{93}$$

in which $\overline{\boldsymbol{n}}=\boldsymbol{F}^{e-1}\boldsymbol{n}$.

As justified earlier with reference to the need to relax the constant wall thickness assumption, we suggest that Eq. (93) is replaced by the following evolution equation:

$$\left.\frac{\partial \dot{\lambda}_{vol}}{\partial t}\right|_{\boldsymbol{X}\ \text{fixed}} = -\frac{\dot{\lambda}_{vol}-\zeta\dot{\lambda}}{t_c} \tag{94}$$

in which t_c is a characteristic time indicating the response time of $\dot{\lambda}_{vol}$ to the change of $\dot{\lambda}$. With the initial condition of $\dot{\lambda}_{vol}|_{t=0}=0$, the solution of Eq. (94) is

$$\dot{\lambda}_{vol}(t)\Big|_{\boldsymbol{X}\ \text{fixed}} = \frac{1}{t_c}\int_0^t e^{(s-t)/t_c}\zeta(s)\dot{\lambda}(s)\mathrm{d}s \tag{95}$$

Thus $\dot{\lambda}_{vol}$ depends on the current state and the history of $\dot{\lambda}$.

To implement Eq. (95) in a numerical scheme, it is useful to retain a linear relationship between $\dot{\lambda}_{vol}$ and $\dot{\lambda}$ in a form similar to Eq. (93). We discuss a discrete format of Eq. (95) with $t=t_{n+1}=t_n+\Delta t$. By using the Eulerian forward differential formulation in Eq. (95), an approximate formulation can be obtained as follows:

$$\dot{\lambda}_{vol}(t_{n+1})\Big|_{\boldsymbol{X}\ \text{fixed}} = \tilde{\zeta}_n\dot{\lambda}\Big|_{t=t_{n+1}},\quad \tilde{\zeta}_n = \left(\frac{\dot{\lambda}_{vol}}{\dot{\lambda}}-\zeta\right)\Big|_{t=t_n} e^{-\Delta t/t_c}+\zeta|_{t=t_n}. \tag{96}$$

Eq. (96) represents the interaction between the isochoric expansion and volumetric growth at macroscopic scale for the living cells. For completeness, $\tilde{\zeta}_n$ is set to be zero for the isolated walls.

4.7. Numerical scheme

Hitherto, an integrative model of *in vivo* cell wall growth is presented with its structure shown in Fig. 7. By assuming that the plastic extension of microfibrils is negligible, the integrative model is sufficiently defined by the yield function of the isochoric expansion in Eq. (44), the flow rule of the isochoric expansion and volumetric growth in Eq. (77), the hardening law in Eq. (85), and the control equation of wall thickness in Eq. (96). It is noted that the rate of effective volumetric deformation, $\dot{\lambda}_{vol}$, is solely controlled by Eq. (96). Thus the yield function, Eq. (46), and the evolution equation, Eq. (63), for the volumetric growth do not appear in the integrative model. The numerical schemes in classical viscoplasticity can be implemented directly in this integrative model.

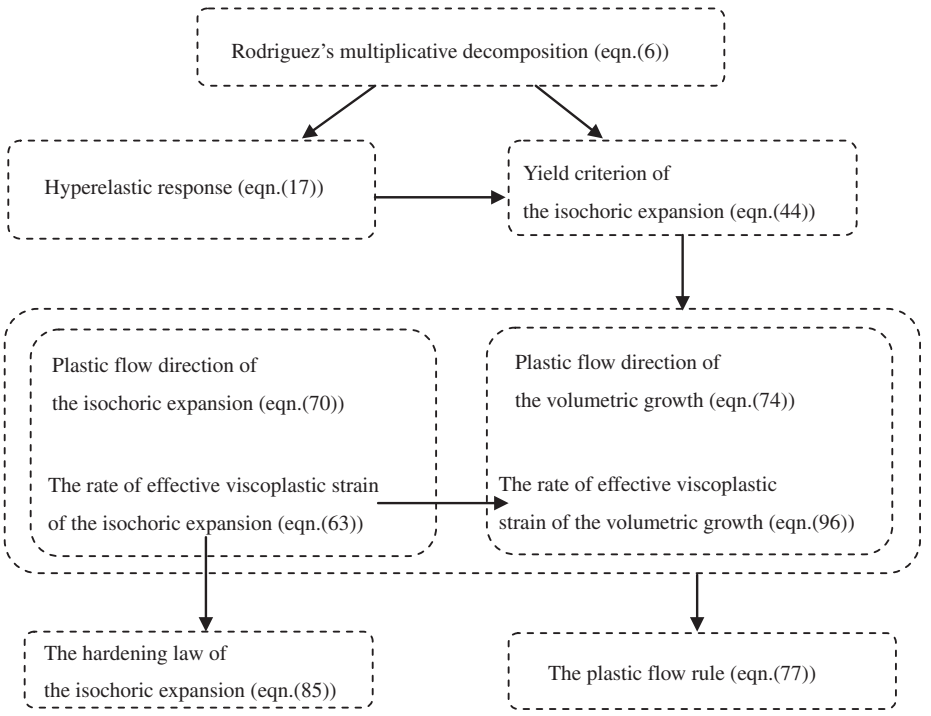

Fig. 7. Structure of the integrative growth model.

4.7.1. Stress update algorithm

Due to the fact that the growth direction usually does not undergo sharp change, the semi-implicit stress update algorithm on $\overline{\mathcal{B}}_t$ suggested by Moran et al. (1990) is adopted in the present numerical implementation. The algorithm, which is a specific return-mapping algorithm, involves two stages; the elastic predictor (trial solution) obtained by freezing the plastic flow, followed by the plastic corrector driven by exactly satisfying Eq. (63) while the total strain and the plastic flow direction are fixed. The algorithm for the present fibre-reinforced model is summarized as follows:

(i) Geometric update from a given incremental displacements $\boldsymbol{u}$

$$\psi_{n+1} = \psi_n + \boldsymbol{u} \tag{97}$$

$$\boldsymbol{F}_{n+1} = \partial\psi_{n+1}/\partial\boldsymbol{X} \tag{98}$$

(ii) Given $\boldsymbol{F}_{n+1}$, $\boldsymbol{F}_n$, $\boldsymbol{F}^g_n$, $\overline{\boldsymbol{S}}_n$, α_n and Δt, update $\boldsymbol{F}^g_{n+1}$, $\overline{\boldsymbol{a}}_{n+1}$, $\overline{\boldsymbol{n}}_{n+1}$, $\overline{\boldsymbol{S}}_{n+1}$ and α_{n+1} by setting

$$\overline{\boldsymbol{R}}_n = \overline{\boldsymbol{R}}^*_n + \tilde{\zeta}_n \overline{\boldsymbol{R}}^*_{vol}(t_n) \tag{99}$$

$$\boldsymbol{F}^g_{n+1} = (1 + \Delta\lambda_n \overline{\boldsymbol{R}}_n)\boldsymbol{F}^g_n \tag{100}$$

$$\boldsymbol{F}^e_{n+1} = \boldsymbol{F}_{n+1}\boldsymbol{F}^{g-1}_{n+1} \tag{101}$$

$$\overline{\boldsymbol{C}}_{n+1} = \boldsymbol{F}^{eT}_{n+1}\boldsymbol{F}^e_{n+1} \tag{102}$$

$$\overline{\boldsymbol{a}}_{n+1} = \boldsymbol{F}^g_{n+1}\boldsymbol{a}_0 \tag{103}$$

$$\overline{\boldsymbol{n}}_{n+1} = \boldsymbol{F}^g_{n+1}\boldsymbol{n}_0 \tag{104}$$

$$\alpha_{n+1} = \alpha_n + (h_1 + h_2\alpha_n)\Delta\lambda_n \tag{105}$$

$$\overline{\boldsymbol{S}}_{n+1} = 2\frac{\partial\Psi(\overline{\boldsymbol{C}}_{n+1}, \overline{\boldsymbol{A}}_{n+1})}{\partial\overline{\boldsymbol{C}}} \tag{106}$$

$$\Delta\lambda_n = \Delta t\frac{\overline{\phi}_{dev}(\overline{\boldsymbol{S}}_{n+1}, \overline{\boldsymbol{a}}_{n+1}, \alpha_{n+1})}{\eta} \tag{107}$$

$$\dot{\lambda}_{vol}(t_{n+1}) = \tilde{\zeta}_n\frac{\Delta\lambda_n}{\Delta t} \tag{108}$$

It is noted that the update algorithm involves a nonlinear equation of the unknown variable $\Delta\lambda_n$. The Newton–Raphson method is used to solve this nonlinear equation. The calculation of the derivative $\mathrm{d}\overline{\phi}_{dev}/d\Delta\lambda_n (= m\phi^{m-1}(\mathrm{d}\phi/d\Delta\lambda_n))$ is the key point for applying the Newton-Raphson method. The expression of $\mathrm{d}\phi/\mathrm{d}\Delta\lambda_n$ is given in Appendix A.

4.7.2. Elasto-viscoplastic tangent modulus

The spatial elasto-viscoplastic tangent modulus consistent with the stress update algorithm is given as (Moran et al., 1990; Belytschko et al., 2001, p. 294)

$$\mathfrak{c}^{\text{elasto-viscoplasticity}} = \frac{\mathfrak{c} - (J^{-1}\mathfrak{c} : \mathrm{sym}\hat{\boldsymbol{r}} + \hat{\boldsymbol{r}}\cdot\boldsymbol{\sigma} + \boldsymbol{\sigma}\cdot\hat{\boldsymbol{r}}^T) \otimes (\overline{\phi}_{\boldsymbol{\tau}} : \mathfrak{c})}{\eta/\Delta t + (\overline{\phi}_{\boldsymbol{\tau}} : \mathfrak{c} : \mathrm{sym}\hat{\boldsymbol{r}}) + \overline{\phi}_{\alpha}} \tag{109}$$

where tensor $\hat{\boldsymbol{r}}$ is defined as

$$\hat{\boldsymbol{r}} = \boldsymbol{F}^{e-T}_{n+1}\overline{\boldsymbol{C}}_{n+1}\overline{\boldsymbol{R}}_n\boldsymbol{F}^g_n\boldsymbol{F}^{g-1}_{n+1}\boldsymbol{F}^{e-1}_{n+1}, \tag{110}$$

tensors $\overline{\phi}_{\boldsymbol{\tau}} = \partial\overline{\phi}_{dev}/\partial\boldsymbol{\tau}$ and $\overline{\phi}_{\alpha} = \partial\overline{\phi}_{dev}/\partial\alpha$ are given in Eqs. (66) and (79), respectively.

It is noted that the term $\tilde{\boldsymbol{a}}$ in the spatial Spencer's deviatoric stress tensor is a unit vector. The derivative of this term with respect to time would involve the asymmetric part (spin) of the spatial velocity gradient $\boldsymbol{L}$, and thus has no contribution to the tangent modulus.

5. Numerical implementation

Loading and unloading by changing the turgor pressure have been used in the experimental study of cell wall mechanical properties. Different components of deformation have occurred and have been mixed together in an *in vivo* growth process to create a complex constitutive response that may blur the interpretation. Proseus and co-workers

(Proseus et al., 1999; Proseus et al., 2000; Proseus and Boyer, 2005, 2006, 2007) presented a series of novel experimental reports on the growth of internode cells of *Chara corallina* as a system in which turgor pressure, temperature and growth interact with each other. Their experimental observations have been widely considered as a clear evidence of viscoplastic behaviour of growing cell wall (Boudaoud, 2003; Dumais et al., 2006). However, no numerical modelling has been reported in the literature to model their experiments. The numerical implementation of the present model aims to cover the major observations in their experimental work. As a phenomenological model based on the common experimental observations and widely accepted hypotheses of general plants, the present constitutive model can be applied to the numerical modelling of other plants if experimental data are available.

The geometry of the model is shown in Fig. 8. The *Chara* cell wall can be considered as a closed cylindrical solid shell with length, L_0, inner radius, $r_I(=0.5\ \text{mm})$, and thickness, $\delta(=10\ \mu\text{m})$ (Toole et al., 2001), subjected to inner pressure P. Microfibrils are aligned transversely in the cell wall. According to the experimental design and observation (Proseus et al., 1999; Proseus and Boyer, 2006) and the theoretical analysis proposed by Boudaoud (2003), the effect of tip growth of cell wall can be ignored when compared to the wall elongation. Thus the model is represented as an open cylindrical wall in the present study. The ends of the cell wall are removed and the turgor pressure applied on the ends is replaced by an equivalent axial stress of value $P(r_I/2\delta)$ applied on the undeformed surface of the two end sections of the open cylindrical wall as shown in Fig. 8.

The constitutive law of the present model is written in a user subroutine (UMAT) in the ABAQUS® FE code. All the numerical case studies are computed by ABAQUS® using a mesh of 600 20-noded 3D quadratic elements, as shown in Fig. 9. Due to the geometry and load symmetry and the fact that the stress is independent of the longitudinal coordinate, the FE model studies only one-eighth of an open-ended thin-walled cylinder with a smaller length $L_0=4$ mm. Symmetric boundary conditions are imposed on the symmetric boundaries. The elongations of the cell walls with their original lengths are obtained by scaling up from the FE solutions.

The elastic and irreversible responses of cell walls interplaying with turgor pressure and temperature reported by Proseus et al. (1999) and Proseus and Boyer (2006) are modelled in the case studies. To the authors' knowledge, this is the first time that all responses have been covered by a single model.

It is worth emphasizing that, although in all of the case studies only the numerical results of longitudinal elongation are reported, our validation is not limited to uniaxial elongation. The components of the anisotropic growth of cell wall in the radial and transverse directions automatically agree well with experimental observation because the major qualitative characteristics of cell growth, i.e. plastic inextensibility of microfibrils and stable wall thickness, are obtained as the result of the flow rule implemented in all case studies.

5.1. Determining material properties from Chara experimental data

Unlike traditional engineering materials, the mechanical properties of the living cell walls are regulated by the active biological mechanisms. For example, it has been reported that the yield stress may change according to the change of turgor pressure to maintain a stable growth (Green et al., 1971). Therefore, it is unlikely that a single set of parameters would be found to fit the data obtained from the available range of experiments. The *Chara* cells used in Proseus'

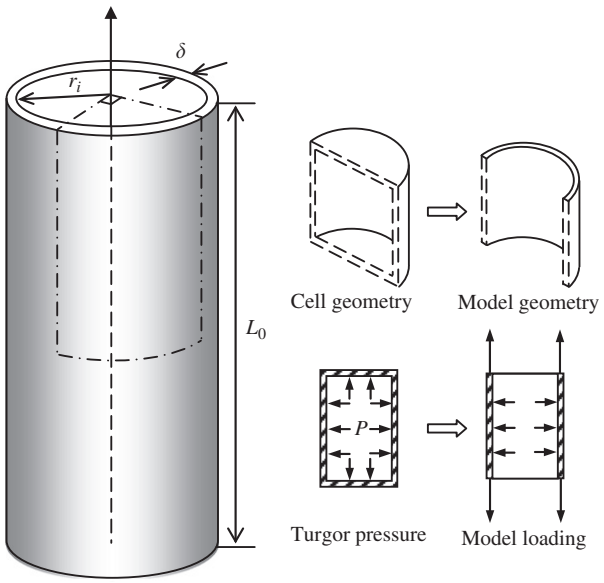

Fig. 8. Geometry of the computational model.

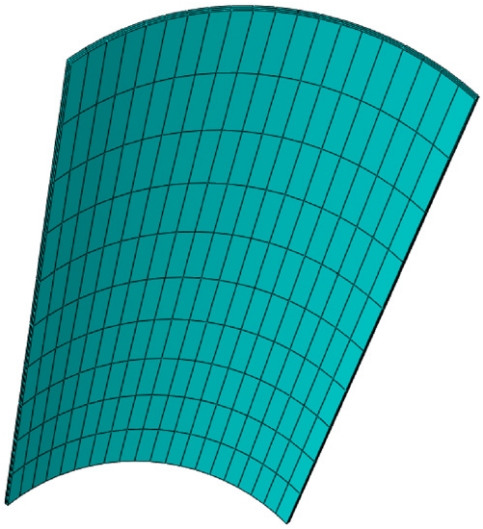

Fig. 9. FE mesh.

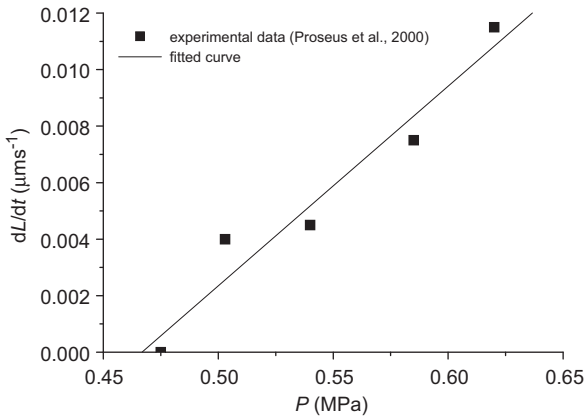

Fig. 10. Relationship between cell growth rate, dL/dt and turgor pressure, P.

experiments varied from one case to the other, so the model parameters may have different values accordingly in the different case studies. But some parameters, e.g. the overstress sensitivity-exponent and the parameters in Arrhenius equation of viscosity, take the same values in all the cases. We report the methods used to estimate all the parameters used in the UMAT subroutine and the (range of) values of the parameters obtained by using these methods.

5.1.1. Overstress sensitivity-exponent

Fig. 10 shows the original experimental data (Proseus et al., 2000, Fig. 13A, temperature=23 °C) and the fitted curve of *Chara* cell growth rate, $\dot{L}$, vs. turgor pressure, P, which is obtained by using the method of least-squares. Here L is the length of the *Chara* cell wall. It is noted that, in the range of turgor pressure covered in the present study (i.e. 0.35–0.6 MPa), the relationship between growth rate and turgor pressure can be represented by a fitted line (see Fig. 10). The intersection of the fitted line and the P axis represents the 'yielding' point ($P \approx 0.47$ MPa in this case). From the yielding point up to the point $P=0.6$ MPa, an assumed linear relationship is reasonable. Therefore, the sensitivity-exponent, m, is taken as 1.0 in the present model. This is consistent with the Lockhart Eq. (1) in which the strain rate is linearly proportional to the turgor pressure in excess of the yield threshold.

For a wider range of turgor pressures, as stated by Proseus et al. (2000), the turgor-growth rate and turgor relationship may be a nonlinear one.

5.1.2. Parameters in the Arrhenius equation of viscosity

Proseus et al. (1999, Fig. 4A) reported the data of normalised growth rate (ratio of growth rate at various temperatures to a growth rate at a reference temperature $T_{ref}=23$ °C) and suggested that growth rate follows the Arrhenius equation. Within a range from 7 °C to 30 °C, the relationship between the growth rate and temperature is suggested to be fitted by

the modified Arrhenius Eq. (64). By using Eq. (64), the natural logarithm of the normalised growth rate, $\ln(\dot{L}/\dot{L}_{\mathrm{ref}})$, has a relationship with temperature T as follows:

$$\ln\frac{\dot{L}}{\dot{L}_{\mathrm{ref}}} = -\frac{Q}{R}\left(\frac{1}{T-T_0}-\frac{1}{T_{\mathrm{ref}}-T_0}\right). \tag{111}$$

Fig. 11 shows the experimental data and theoretical curve of $\ln(\dot{L}/\dot{L}_{\mathrm{ref}})$ vs. $1/T$ fitted to the experimental data by using the method of least-squares. The parameters of the fitted curve are $Q/R=50.0$ and $T_0=0$ °C, respectively.

5.1.3. Summary of the model parameters and estimation methods

In Appendix B we discuss the analytical solution of the small strain elasto-viscoplastic deformation of a closed cylindrical shell subjected to inner pressure P. The parameters such as Young's modulus E, dynamic yield thresholds $(1+h)Y_1$ and $(1+h)Y_2$, and viscosity η can be estimated by using this analytical solution. Table 2 gives the summary of the model parameters used in the FE analysis and the methods used for parameter estimation. Given experimental data, an initial estimation of model parameters can be obtained by using the values and methods provided in Table 2. To obtain better fitting to the experimental data, FE simulation is needed to try and optimise the parameter estimation. Because

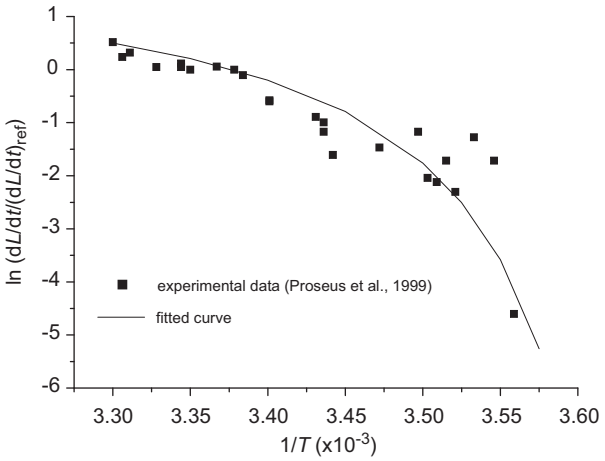

Fig. 11. Relationship between the normalised growth rate and temperature.

Table 2
Model parameters and estimation.

Hyperelasticity	E (Young's modulus of the cell wall matrix)	Range from 1.5 to 5.0 GPa (converted from Fig. 6 by Proseus et al. (1999) according to the geometry of wall). Can be estimated more precisely if experimental data for the elastic response is available
	v (Possion's ratio of the cell wall matrix)	$v=0.3$ estimated according to the hypothesis that the cell wall is a porous material (Proseus and Boyer, 2005)
	κ_1, κ_2 (microfibrils elastic parameters)	$(\kappa_1=\mu(=E/(2(1+v))$, $\kappa_2=1.0$. Estimated by using Young's modulus of single cellulose microfibrils, 150.0 GPa (Iwamoto et al. 2009), and assuming the volume fraction of microfibrils to be about 1–3%
Viscoplasticity	Y_1, Y_2 (*static* yield parameters)	Range from 3.5 to 7.0 MPa (converted from turgor pressure threshold from 0.2 to 0.4 MPa (Cosgrove, 1986)) It is noted that, if the reference configuration ($t=0$) has an unknown history of growth during the time interval $t\in(-\infty,0]$, values of Y_1 and Y_2 actually are the *dynamic* yield thresholds $(1+h|_{t=0})Y_1$ and $(1+h|_{t=0})Y_2$ with an unknown $h|_{t=0}$. The dynamic yield thresholds can be estimated by using the method suggested in Appendix B if experimental data of growth rates under two different turgor pressures are available. Our FE simulation shows that the dynamic yield thresholds range from 6.0 to 9.5 MPa which are higher than the corresponding static thresholds
	η (or η_0) (viscosity)	Range from 10^{10} to 10^{13} Pa s, estimated from the experimental data of growth (curves of rate of elongation vs. time which were reported by Proseus et al. (1999, 2006)) by using the method suggested in Appendix B
	h_1, h_2 (hardening parameters)	$h_1\approx 20.6$ and $h_2\approx 20.0$. Obtained by numerical experiments to fit the experimental data of the long-term growth (Proseus and Boyer, 2006, Fig. 4). For the experimental data of a short-term growth without obvious hardening, h_1 can be smaller than 20.6 to obtain better fitting
	Q (activation energy)	$Q=50.0R$ (R is the gas constant) and $T_0=0$ °C.
	T_0 (model parameter)	Estimation method reported in Section 5.1.2
	t_c (characteristic time)	$t_c=10s$. Estimated according to the experimental data (Proseus et al., 1999, Fig. 2) where a time interval of 10 s was short enough to keep natural growth negligible

different internode cells of *Chara corallina* were used in different experiments, the values of the parameters may be different from one case study to the other.

5.2. Case studies of the cell wall growth

5.2.1. Case study 1: components of cell elongation: change in length of a cell wall when turgor pressure P is rapidly changed with P pulses

In this case, the cell solution was injected using a pressure probe to increase P by 0.04 MPa in 10 s. P was kept at the new level for 10 s and then returned to the original level (0.526 MPa) in 10 s. This process was repeated twice with 2 min between each pulse as shown in Fig. 12(a). The P pulse produced both an elastic response and *in vitro* growth as reported by Proseus et al. (1999, Fig. 2). Whether the *in vitro* growth is viscoplastic or viscoelastic is still an open question (Schopfer, 2006; Suslov and Verbelen, 2006). However, in the time scale considered in the experiment, the *in vitro* growth reported by Proseus et al. may be considered as a viscoplastic behaviour since it was clearly irreversible even long after the P pulse was removed.

The cell is initially 13 mm long. Young's modulus of the cell wall matrix is chosen as $E=3.0$ GPa and Possion's ratio as $\nu=0.3$. The two parameters κ and μ in the hyperelastic response of the cell wall matrix are calculated by $\kappa=E/(3(1-2\nu))$ and $\mu=E/(2(1+\nu))$, respectively. The parameters of the microfibrils' elastic response are set as $\kappa_1=\mu$ and $\kappa_2=1.0$. For the viscoplastic response, the yield parameters, Y_1 and Y_2, are set as $Y_1=Y_2=9.125$ MPa. The viscosity is 1.26875×10^{11} Pa s. Hardening parameters are taken as $h_1=20.6$ and $h_2=20.0$. For the purpose of demonstration, the fitting process to obtain the values of parameters was conducted manually in each case study in order to achieve a subjectively good fit; more sophisticated least-squares methods could be employed.

The FE solutions are shown in Fig. 12(b) compared with the experimental data (Proseus et al., 1999, Fig. 2B). The results indicate that there are three components in the elongation of cell wall: (1) *in vivo* growth, (2) *in vitro* growth, and (3) elastic response.

In Fig. 12(b), Part ① of the elongation is the *in vivo* growth under constant turgor pressure. During this stage, $\dot{\lambda}_{vol}$ exactly matches $\dot{\lambda}$ to maintain a constant wall thickness. Part ② of the elongation is an irreversible deformation mainly attributed to the *in vitro* growth produced by the P pulse although the *in vivo* growth makes its contribution as well. As the characteristic time t_c is set large enough by comparison with the time interval (30 s) of the P pulse, the change of $\dot{\lambda}_{vol}$ lags far behind the change of $\dot{\lambda}$ during the *in vitro* growth (result not shown). Thus, although both are irreversible growth, Part ① and part ② of the elongation can be distinguished from each other by whether the exact match between $\dot{\lambda}_{vol}$ and $\dot{\lambda}$ is violated. Finally, Fig. 12(b) shows part ③ of the elongation which is an elastic response.

It is noted that neither the elastic model nor the viscous model alone can represent the experimental observation in this case study. Moreover, other existing models using the assumption of constant wall thickness cannot distinguish the rapid *in vitro* growth from the *in vivo* growth in this experiment.

5.2.2. Case study 2: effects of turgor pressure changes: P steps for growing young cells and mature cells

Case study 1 has shown that a mix of *in vivo* growth and *in vitro* growth occurs under the rapid P pulses. To study the effect of turgor pressure change on *in vivo* growth, in the reported experiment (Proseus et al., 1999, Fig. 3A) the P steps were generated with a pressure probe by removing or injecting cell solution without changing the environment of the cell as shown in Fig. 13(a) for a young cell. The original turgor pressure is 0.5 MPa at stage ①. The turgor pressure decreases from its original level down to 0.46 MPa at stage ②. After keeping at this level for 30 min, the turgor pressure increases to its original level at stage ③.

The cell is initially 12 mm long. Young's modulus of the cell wall matrix is chosen as $E=1.65$ GPa and Possion's ratio as $\nu=0.3$. The parameters of the elastic response of microfibrils are set as $\kappa_1=\mu$ and $\kappa_2=1.0$. For the viscoplastic response,

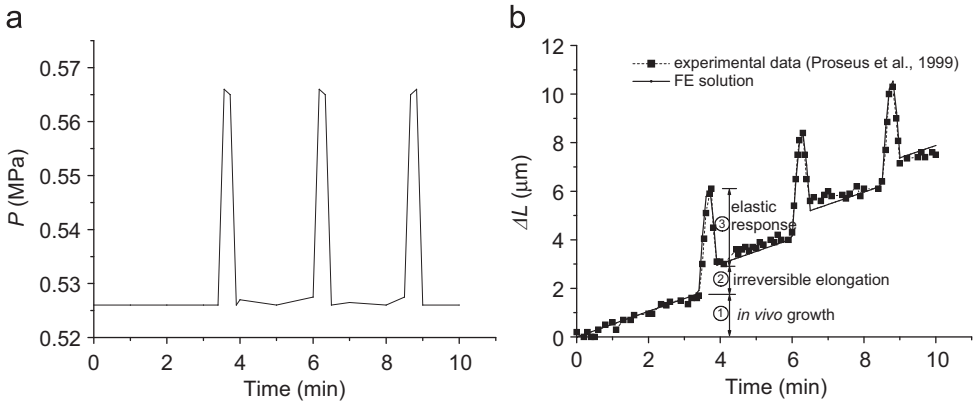

Fig. 12. Effects of P pulses: (a) P pulses superimposed on normal turgor pressure, and (b) cell elongation.

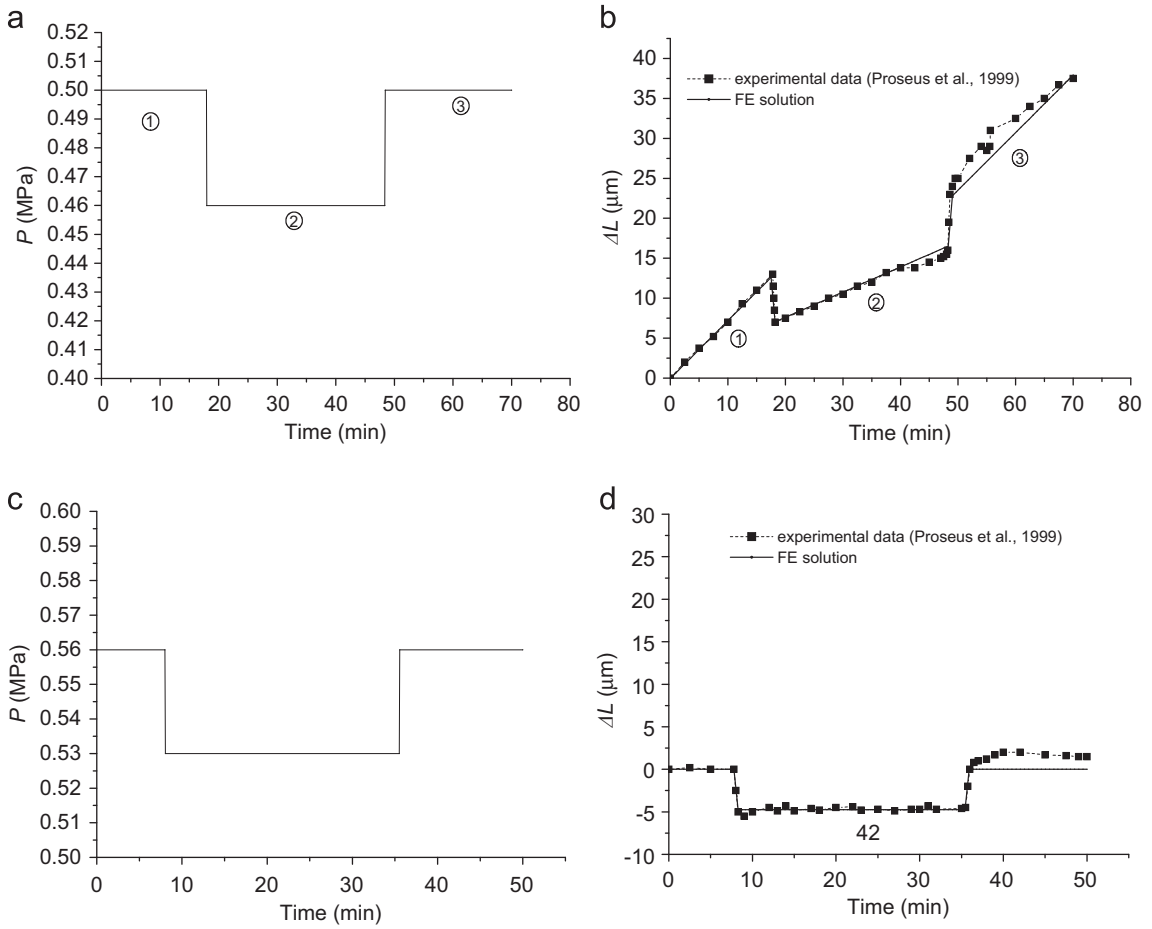

Fig. 13. The effect of turgor pressure change on the deformation of young and mature cells. (a) Turgor pressure vs. time for a young cell, (b) length change vs. time for a young cell, (c) turgor pressure vs. time for a mature cell, and (d) length change vs. time for a mature cell.

the yield parameters, Y_1 and Y_2, are set as $Y_1=Y_2=6.125$ MPa. The viscosity is 9.677745×10^{12} Pa s. Hardening parameters are taken as $h_1=20.6$ and $h_2=20.0$.

The FE solutions are shown in Fig. 13(b) compared with the experimental data (Proseus et al., 1999; Fig. 3B). The main characteristics of the experimental observation are captured by the numerical solution, i.e. (a) instantaneous elastic response for P steps and (b) change of growth rate at different P levels.

In contrast to case study 1 in which the P pulse was short enough to keep the *in vivo* growth negligible, in this case study the turgor pressure was kept at the new levels long enough to indicate the relationship between turgor pressure and *in vivo* growth. Corresponding to the changes of turgor pressure, the *in vivo* growth rate decreased from stage ① to stage ②, and then resumed the original growth rate at stage ③. Thus the experimental observation indicates that *in vivo* growth rate can be regulated by turgor pressure. This observation is the experimental foundation of the mechanical modelling of cell wall growth. However, we should bear in mind that in essence growth is controlled by the biological mechanisms and the turgor pressure is just a passive driving force. As shown in the following study for a mature cell, the change of turgor pressure cannot alter the absence of growth in a mature cell.

FE solutions for a mature cell are presented in Fig. 13(c) and (d). Young's modulus of the cell wall matrix is chosen as $E=2.0$ GPa which is higher than that of a young cell as reported in Proseus et al. (1999, Fig. 8C and D). To represent the non-growth behaviour of a mature cell, there are the two options in the present model: either raising the yield threshold or raising the viscosity. The two options, although involving different mechanisms from the point of view of solid mechanics, are capable of simulating the absence of cell wall loosening in a mature cell. Thus a higher yield threshold is set as $Y_1=Y_2=10$ MPa for a mature cell but the viscosity is kept the same as for a young cell. The numerical results show that the mature cell responds mainly in an elastic mode.

5.2.3. *Case study 3: temperature effects*

The Arrhenius equation of viscosity is suggested in Eq. (64) and the values of activation energy, Q, and parameter T_0 are calculated from the experimental data shown in Fig. 11. In order to verify this equation and the values of the parameters,

in this case study the turgor pressure is fixed but the temperature has a temporal change as shown in Fig. 14(a). The data of turgor pressure and temperature are adopted from the experimental results of Proseus and Boyer (2006, Fig. 7A and C).

The initial length of the cell is 12 mm. Young's modulus of the cell wall matrix is chosen as $E=2.5$ GPa and Possion's ratio as $\nu=0.3$. The parameters of the elastic response of microfibrils are set as $\kappa_1=\mu$ and $\kappa_2=1.0$. The yield parameters, Y_1 and Y_2, are set as $Y_1=Y_2=6.25$ MPa. The viscosity parameter η_0 in Eq. (64) is 2.7926×10^{11} Pa s. Hardening parameters are taken as $h_1=2.0$ and $h_2=20.0$. Turgor pressure P is a constant 0.47 MPa.

The FE solutions are shown in Fig. 14(b) together with the corresponding experimental data (Proseus and Boyer, 2006, Fig. 7B). The results indicate that the model can accurately represent the effect of temperature on the cell growth.

5.2.4. Case study 4: separating elastic deformation from growth

In the experiments involving turgor pressure change by removal or injection of cell content or water, the growth occurs simultaneously with stress-induced elastic deformation. The idea of separating the elastic deformation from growth is based on the fact that at lower temperatures, e.g. 7 °C, growth vanishes but the elastic response is the same as at the higher temperature, e.g. 23 °C. Thus by subtracting the deformation at the lower temperature from the total deformation at the higher temperature, the growth at the higher temperature can be obtained.

In this case study, step changes in turgor pressure P (P steps) shown in Fig. 15(a) (Proseus et al., 1999, Fig. 8A) are applied to cause instantaneous elastic deformation and change of growth rates. The responses of the cell wall when subjected to P steps at two different temperatures, 23.7 °C and 7.3 °C, are studied.

The initial length of the cell is 12 mm. Young's modulus of the cell wall matrix is chosen as $E=4.15$ GPa and Possion's ratio as $\nu=0.3$. The parameters of the elastic response of microfibrils are set as $\kappa_1=\mu$ and $\kappa_2=1.0$. The yield parameters, Y_1 and Y_2, are set as $Y_1=Y_2=8.0$ MPa. The viscosity parameter η_0 in Eq. (64) is 3.71739×10^{12} Pa s. Hardening parameters are taken as $h_1=20.6$ and $h_2=20.0$.

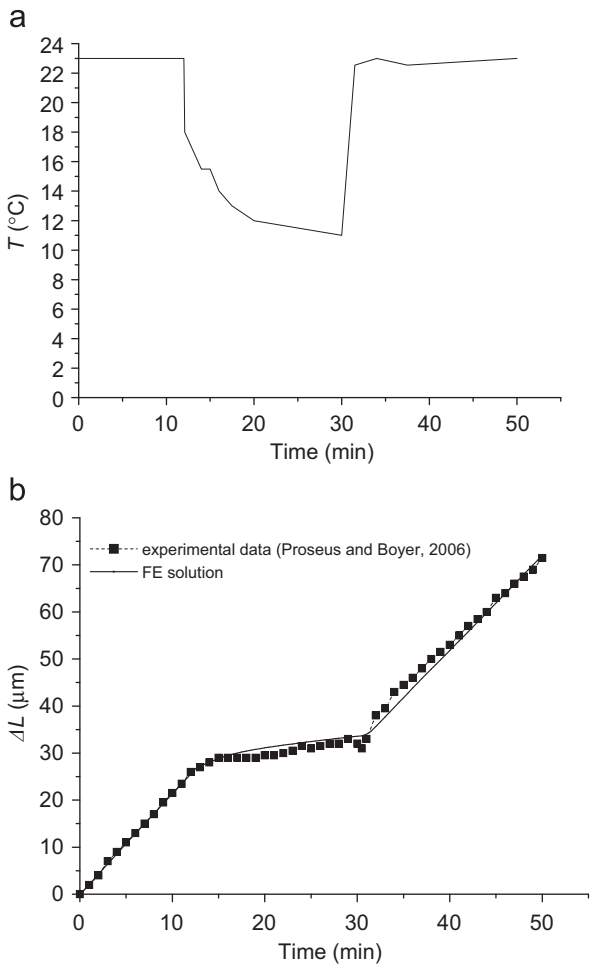

Fig. 14. The effect of temperature change on the growth of young cell. (a) temperature vs. time and (b) length change vs. time.

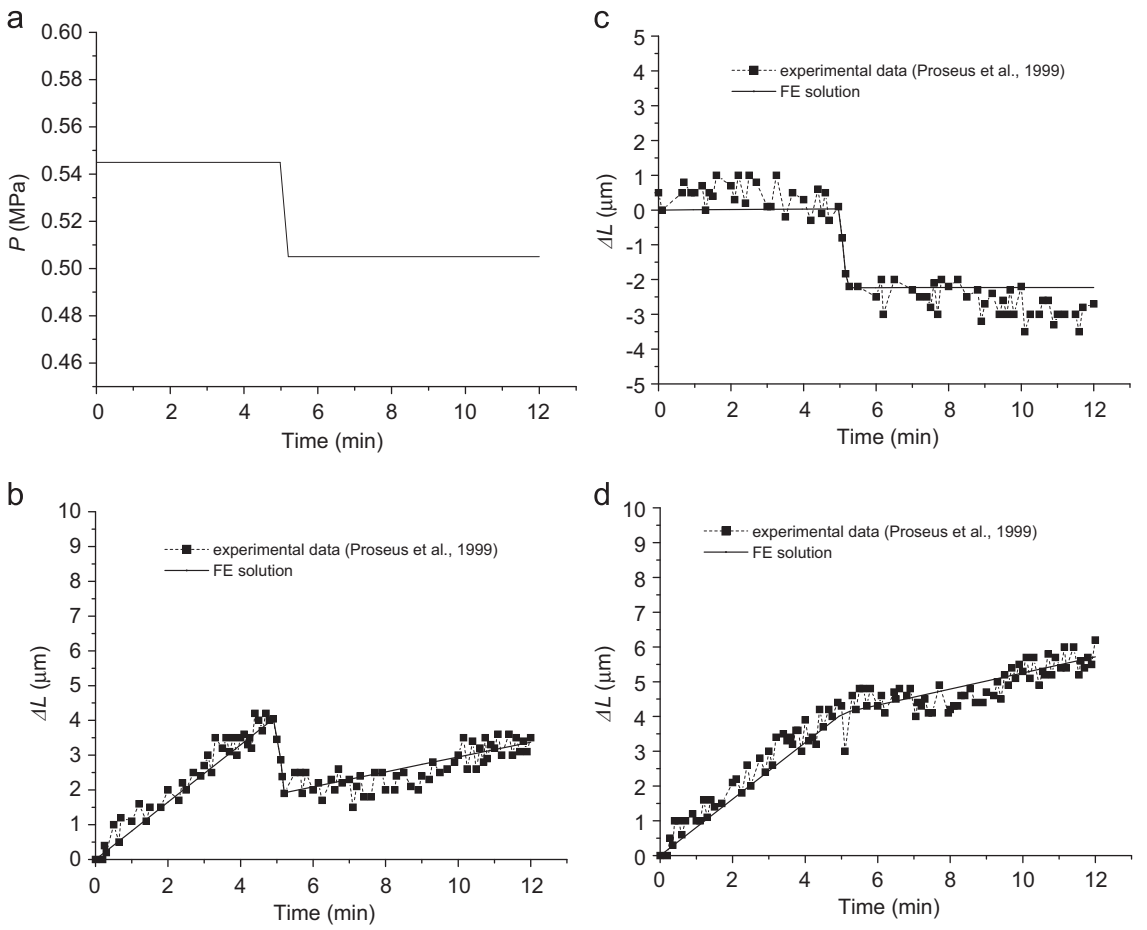

Fig. 15. Growth interaction with turgor pressure and temperature. (a) turgor pressure vs. time, (b) length change vs. time at 23.7 °C, (c) length change vs. time at 7.3 °C, and (d) growth vs. time.

The FE solutions are shown in Fig. 15(b) and (c) together with the corresponding experimental data (Proseus et al., 1999, Fig. 8B and C) for comparison. The growth which is obtained by subtracting deformation at 7.3 °C from that at 23.7 °C, is shown in Fig. 15(d) together with the corresponding experimental data (Proseus et al., 1999, Fig. 8D). The FE solutions show that the present model can represent the experimental observation of the cell wall growth as a 'turgor pressure–temperature' interaction system.

5.2.5. *Case study 5: long-term growth*

Proseus and Boyer (2006) reported the temporal data of growth of a *Chara* living cell and an isolated wall subjected to constant turgor pressure during a time interval of about 20 h. The elongation against time curve of the living cell showed an early stage of fast growth and a second stage of slower but sustainable growth. By contrast, the isolated wall showed a short early stage of fast growth following by a second stage with negligible growth. To the authors' knowledge, modelling of this kind of experimental observation has not been reported elsewhere.

The model parameters for the living cell are given as follows. The initial length of the cell is 12 mm. Young's modulus of the cell wall matrix is chosen as $E=2.5$ GPa and Possion's ratio as $\nu=0.3$. The parameters of the microfibrils elastic response are set as $\kappa_1=\mu$ and $\kappa_2=1.0$. The yield parameters, Y_1 and Y_2, are set as $Y_1=Y_2=5.9$ MPa. The viscosity parameter η is 2.0253×10^{12} Pa s. Turgor pressure P is a constant 0.5 MPa. Hardening parameters are taken as $h_1=20.6$ and $h_2=20.0$. For the isolated wall, all the parameters are the same as those of the living cell except that $h_1=66.0$ and $h_2=0.0$.

It is noted that Zhu and Boyer (1992) also reported earlier their observations on similar experiments. In contrast to the observation reported by Proseus and Boyer (2006), there was no perceivable hardening taking place in Zhu and Boyer's experiment. To model Zhu and Boyer's experimental observation, the viscosity parameter η is taken as 1.4536×10^{13} Pa s, and hardening parameter h_2 as 200.0. The initial length of the cell is 21 mm. All other parameters have the same values as those used in modelling the Proseus and Boyer's experiment (2006).

The numerical FE solutions are shown in Fig. 16 together with the corresponding experimental data (Proseus and Boyer, 2006, Fig. 4; Zhu and Boyer, 1992, Fig. 3(D)). In Fig. 16, the growth of the living cells shows sustainable growth with a

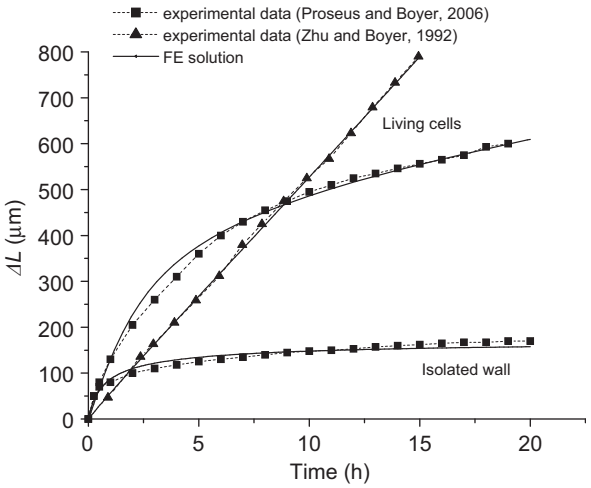

Fig. 16. Long-term growth of the living cells and isolated wall.

steady growth rate either after a transfer from a stage ① of fast elongation to a stage ② of slower elongation or without any transfer. By contrast, the isolated wall stops growing after a very short stage of fast growth. The FE solutions show that the present model can represent these experimental observations by using the simple hardening law from Eq. (85).

The difference between the experiments reported by Zhu and Boyer (1992) and Proseus and Boyer (2006) may be explained by the environmental conditions of the cells. In Proseus and Boyer's experiment, the cell might have been kept under suboptimal conditions leading to a declining growth rate. Bearing in mind that our hardening law (85) is based on the mechanism of interplay between cell wall and its environment, our model of living cell growth represents the effect of the environment on different experiments through the plastic hardening law.

It is noted that, to represent the decrease of growth rate in a long-term growth, there is a so-called multi-net growth model which holds that, as the cell elongates, microfibrils rotate passively, becoming progressively aligned towards the longitudinal axis to strengthen the cell wall in that direction (except those that are precisely transverse) (Marga et al., 2005). Thus stiffening in the multi-net growth model was based on a fibre-dominated mechanism, essentially different from the matrix-dominated mechanism in the hardening law of the present model. The multi-net model seems unable to account for the observations of growth of living cells reported by Proseus and Boyer (2006) because no re-orientations of microfibrils were reported and Proseus et al. proposed a hardening mechanism based on molecular mechanisms of cross-links (Proseus et al., 1999; Proseus and Boyer, 2006) consistent with the present hardening law. It is unlikely that a cell that has grown from an initial length of a few millimetres to a length of 12 mm and that potentially still has a few tens of millimetres to grow before reaching its full length would undergo rapid wall stiffening resulting from microfibrils rotation at the time when an experiment is being performed. Therefore, we consider that a matrix-dominated viscoplastic hardening, rather than a microfibrils-dominated multi-net hypothesis, is sufficient to account for the hardening in the present numerical study.

Moreover, a multi-net model, which predicts that if the initial alignment of the microfibrils is not perfectly aligned in the transverse direction, the rotation of microfibrils towards the longitudinal direction will reduce the growth rate of cell wall, which contradicts the prevailing biological hypothesis that the build-up of shear during microfibrils rotation (slippage) should favour the wall expansion (Cosgrove, 1986). Again, the microfibrils-dominated multi-net hypothesis shows inconsistency with the matrix-dominated mechanism of wall expansion. This contradiction can be addressed straightforwardly by using the present model. The driving force of wall expansion in our model is not the loosely-defined shear but the Spencer's deviatoric stress as defined in Eqs. (38) and (39). Spencer's deviatoric stress indicates that there is no driving force of growth in the microfibrils direction (Eqs. (40) and (41)). Therefore, even though there may be a build-up of shear during growth, the driving force of expansion would decrease as the microfibrils rotate towards a direction aligning with the longitudinal direction, which addresses the contradiction raised by the multi-net model.

6. Conclusions

How the plant expands its cell walls to grow while maintaining sufficient strength and the role of mechanics in this expansive growth are the central challenges in integrative biology. Constitutive modelling is the vital step to understand and analyse this problem. A unique characteristic of the constitutive behaviours in the cell wall growth by comparison with engineering materials, such as metals, is the indispensable interplay at different scales between the turgor-pressure-driven expansion and the new material deposition.

From the point of view of bottom-up design, mechanism-based modelling using microstructural properties is an important method to understand cell wall growth. However, considering the complexity of the microstructure of cell wall, whose details are largely unknown to date, phenomenological modelling is an indispensable method for understanding the role of mechanics at the cell and tissue scales. Different from empirical modelling which is based on fitting data, our phenomenological constitutive modelling is based on a rigorous framework of solid mechanics, deliberately guided by the existing biological hypotheses and experimental observations, and can provide insight into the role of mechanics in cell wall growth at cell scale.

A fibre-reinforced hyperelastic–viscoplastic model is presented to cover some important characteristics of the expansive growth of the cell walls. The kinematics of multiplicative decomposition of the deformation gradient is introduced into the model to bridge the gap between cell wall modelling and plasticity theory. The cellulose microfibrils are considered explicitly in the anisotropic model to represent their roles in regulating specific growth directions. Unlike existing elastic or viscous models in which the tensile modulus of cellulose microfibrils must be far greater than that of the wall matrix, the present model avoids this loosely defined constraint by introducing an assumption of decomposition of growth based on experimental observations. Using the decomposition of growth, we suggest a set of yield functions and a flow rule to clarify the mechanical mechanisms of the *in vivo* anisotropic growth of cell wall. The interplays between expansive growth and new material deposition are discussed at both molecular and macroscopic scales. The interplay model at a molecular scale yields a mechanism-based hardening law which distinguishes a living cell from an isolated wall without using biological variables. This sheds a new light into the modelling of interplay between wall-yielding and wall-stiffening which play a key role in regulating a sustainable growth. The effect of temperature is also taken into account in the model by using an Arrhenius equation.

The model is formulated in a finite strain format and a numerical scheme is presented, which is applicable to nonlinear FE analysis. The model is incorporated in a user-subroutine in the ABAQUS® FE code, and applied to five case studies reflecting different aspects of *Chara* cell growth. The results show that the model is capable of describing the interplay among growth, turgor pressure and temperature, as justified by the FE solutions which show good fitting of experimental data. As a phenomenological model representing general characteristics of the cell walls, the present constitutive model can be applied to the numerical modelling of other plants if experimental data are available.

Acknowledgement

This work was conducted in the Centre for Plant Integrative Biology, University of Nottingham, U.K., which is jointly funded by the BBSRC and EPSRC (BB/D0196131/1) as part of their Systems Biology Initiative.

Appendix A: The derivation of $\partial\phi/\partial\Delta\lambda_n$

Let χ be an entity standing for tensor, vector or scalar. By taking derivative of Eq. (56) with respect to χ we obtain

$$\frac{\partial\theta}{\partial\chi}=\vartheta_1\frac{\partial\bar{J}_1}{\partial\chi}+\vartheta_2\frac{\partial\bar{J}_2}{\partial\chi}+\vartheta_h\frac{\partial h}{\partial\chi} \tag{A1}$$

where

$$\vartheta_1=(Y_1^2(\theta-Y_2^2)^2/\vartheta_D),\quad \vartheta_2=Y_2^2(\theta-Y_1^2)^2/\vartheta_D,\quad \vartheta_h=-(\theta-Y_1^2)^2(\theta-Y_2^2)^2/\vartheta_D \tag{A2}$$

in which

$$\vartheta_D=2\{(1+h)(\theta-Y_1^2)(\theta-Y_2^2)(2\theta-Y_1^2-Y_2^2)-\bar{J}_1Y_1^2(\theta-Y_2^2)-\bar{J}_2Y_2^2(\theta-Y_1^2)\}. \tag{A3}$$

Using the chain rule and substituting Eq. (A1) into the derivative of the distance function ϕ with respect to χ yields

$$\frac{\partial\phi}{\partial\chi}=\left(\frac{\partial\phi}{\partial\bar{J}_1}+\vartheta_1\frac{\partial\phi}{\partial\theta}\right)\frac{\partial\bar{J}_1}{\partial\chi}+\left(\frac{\partial\phi}{\partial\bar{J}_2}+\vartheta_2\frac{\partial\phi}{\partial\theta}\right)\frac{\partial\bar{J}_2}{\partial\chi}+\vartheta_h\frac{\partial\phi}{\partial\theta}\frac{\partial h}{\partial\chi} \tag{A4}$$

in which

$$\frac{\partial\phi}{\partial\bar{J}_1}=\frac{\theta^2}{2\phi(Y_1^2-\theta)^2},\quad \frac{\partial\phi}{\partial\bar{J}_2}=\frac{\theta^2}{2\phi(Y_2^2-\theta)^2},\quad \frac{\partial\phi}{\partial\theta}=\frac{\phi}{\theta}+\frac{\theta^2}{\phi}\left(\frac{\bar{J}_1}{(Y_1^2-\theta)^3}+\frac{\bar{J}_2}{(Y_2^2-\theta)^3}\right). \tag{A5}$$

With the general Eq. (A4), the remaining work is to calculate the explicit expressions of $\partial\bar{J}_1/\partial\chi$, $\partial\bar{J}_2/\partial\chi$ and $\partial h/\partial\chi$ with respect to a given entity χ.

The following discussion is restricted to the case in which $\chi=\Delta\lambda_n$. The expression of $\partial h/\partial\Delta\lambda_n$ is trivial considering the hardening law Eq. (78) and the update format in Eq. (105). So only $\partial\bar{J}_1/\partial\Delta\lambda_n$ and $\partial\bar{J}_2/\partial\Delta\lambda_n$ are discussed here. In the following calculation, all the variables refer to discrete time t_{n+1}.

By taking the derivative of Eqs. (42) and (43) with respect to $\Delta\lambda_n$, we obtain

$$\frac{\partial \bar{J}_1}{\partial \Delta\lambda_n} = \frac{2}{\lambda_{\boldsymbol{a}}}\frac{\partial \overline{\boldsymbol{a}}}{\partial \Delta\lambda_n}\cdot(\overline{\boldsymbol{C}}\overline{\boldsymbol{S}}^{DEV}\overline{\boldsymbol{C}}\overline{\boldsymbol{S}}^{DEV}\overline{\boldsymbol{C}}\overline{\boldsymbol{a}}) + \frac{2}{\lambda_{\boldsymbol{a}}}\overline{\boldsymbol{a}}\cdot\left(\frac{\partial \overline{\boldsymbol{C}}}{\partial \Delta\lambda_n}\overline{\boldsymbol{S}}^{DEV}\overline{\boldsymbol{C}}\overline{\boldsymbol{S}}^{DEV}\overline{\boldsymbol{C}}\overline{\boldsymbol{a}}\right) + \frac{2}{\lambda_{\boldsymbol{a}}}\overline{\boldsymbol{a}}\cdot\left(\overline{\boldsymbol{C}}\frac{\partial \overline{\boldsymbol{S}}^{DEV}}{\partial \Delta\lambda_n}\overline{\boldsymbol{C}}\overline{\boldsymbol{S}}^{DEV}\overline{\boldsymbol{C}}\overline{\boldsymbol{a}}\right) + \frac{1}{\lambda_{\boldsymbol{a}}}\overline{\boldsymbol{a}}\cdot\left(\overline{\boldsymbol{C}}\overline{\boldsymbol{S}}^{DEV}\frac{\partial \overline{\boldsymbol{C}}}{\partial \Delta\lambda_n}\overline{\boldsymbol{S}}^{DEV}\overline{\boldsymbol{C}}\overline{\boldsymbol{a}}\right) \tag{A6}$$

and

$$\frac{\partial \bar{J}_2}{\partial \Delta\lambda_n} = 2\frac{\partial \overline{\boldsymbol{C}}}{\partial \Delta\lambda_n} : \left[\overline{\boldsymbol{S}}^{DEV}\overline{\boldsymbol{C}}\overline{\boldsymbol{S}}^{DEV}\right] + 2\overline{\boldsymbol{C}} : \left[\overline{\boldsymbol{S}}^{DEV}\overline{\boldsymbol{C}}\frac{\partial \overline{\boldsymbol{S}}^{DEV}}{\partial \Delta\lambda_n}\right] \tag{A7}$$

in which the expressions for $\partial\overline{\boldsymbol{a}}/\partial\Delta\lambda_n$, $\partial\overline{\boldsymbol{C}}/\partial\Delta\lambda_n$ and $\partial\overline{\boldsymbol{S}}^{DEV}/\partial\Delta\lambda_n$ need to be worked out. The fact that the stretch of fibre, $\lambda_{\boldsymbol{a}}$ (defined in Eq. (5)), is fixed during the plastic corrector stage is used in the process of calculation. This fact is the natural result of the plastic inextensibility assumption of the microfibrils.

First, by using Eqs. (100) and (103), $\partial\overline{\boldsymbol{a}}/\partial\Delta\lambda_n$ is obtained as

$$\frac{\partial \overline{\boldsymbol{a}}}{\partial \Delta\lambda_n} = \overline{\boldsymbol{R}}_n\boldsymbol{a}_0. \tag{A8}$$

Second by using Eqs. (100)–(102), the expression of $\partial\overline{\boldsymbol{C}}/\partial\Delta\lambda_n$ is obtained as

$$\frac{\partial \overline{\boldsymbol{C}}}{\partial \Delta\lambda_n} = -[\Delta\boldsymbol{F}_n^g]^{-T}(\overline{\boldsymbol{R}}_n[\Delta\boldsymbol{F}_n^g]^{-T}\overline{\boldsymbol{C}}_{n+1}^{trial} + \overline{\boldsymbol{C}}_{n+1}^{trial}[\Delta\boldsymbol{F}_n^g]^{-1}\overline{\boldsymbol{R}}_n)[\Delta\boldsymbol{F}_n^g]^{-1} \tag{A9}$$

where the tensor $\overline{\boldsymbol{C}}_{n+1}^{trial}$ is defined as

$$\overline{\boldsymbol{C}}_{n+1}^{trial} = \boldsymbol{F}_n^{g-T}\boldsymbol{C}_{n+1}\boldsymbol{F}_n^{g-1}. \tag{A10}$$

It is noted that in the return-mapping algorithm, the total strain C_{n+1} on the right-hand side of Eq. (A10) is computed from the elastic trial solution (elastic predictor) and is fixed during the plastic corrector stage. It can be proved that $\overline{\boldsymbol{C}}_{n+1}^{trial}$ is exactly the elastic trial solution of the elastic right Cauchy–Green tensor.

Third, the derivative of Spencer's deviatoric stress tensor with respect to $\Delta\lambda_n$ is

$$\begin{aligned}\frac{\partial \overline{\boldsymbol{S}}^{DEV}}{\partial \Delta\lambda_n} = {} & \frac{\partial \overline{\boldsymbol{S}}}{\partial \Delta\lambda_n} + \frac{1}{2}\left\{\frac{1}{\lambda_{\boldsymbol{a}}}\frac{\partial \|\overline{\boldsymbol{S}}\|_{\overline{\boldsymbol{a}}}}{\partial \Delta\lambda_n} - \frac{\partial \mathrm{Tr}\overline{\boldsymbol{S}}}{\partial \Delta\lambda_n}\right\}\overline{\boldsymbol{C}}^{-1} + \frac{1}{2}\left\{\frac{1}{\lambda_{\boldsymbol{a}}}\|\overline{\boldsymbol{S}}\|_{\overline{\boldsymbol{a}}} - \mathrm{Tr}\overline{\boldsymbol{S}}\right\}\frac{\partial \overline{\boldsymbol{C}}^{-1}}{\partial \Delta\lambda_n} + \frac{1}{2}\frac{1}{\lambda_{\boldsymbol{a}}}\left\{-\frac{3}{\lambda_{\boldsymbol{a}}}\frac{\partial \|\overline{\boldsymbol{S}}\|_{\overline{\boldsymbol{a}}}}{\partial \Delta\lambda_n} + \frac{\partial \mathrm{Tr}\overline{\boldsymbol{S}}}{\partial \Delta\lambda_n}\right\}\overline{\boldsymbol{A}} \\ & + \frac{1}{2}\frac{1}{\lambda_{\boldsymbol{a}}}\left\{-\frac{3}{\lambda_{\boldsymbol{a}}}\|\overline{\boldsymbol{S}}\|_{\overline{\boldsymbol{a}}} + \mathrm{Tr}\overline{\boldsymbol{S}}\right\}\frac{\partial \overline{\boldsymbol{A}}}{\partial \Delta\lambda_n}.\end{aligned} \tag{A11}$$

The expressions of (1) $\partial\overline{\boldsymbol{S}}/\partial\Delta\lambda_n$, (2) $\partial\overline{\boldsymbol{A}}/\partial\Delta\lambda_n$, (3) $\partial\overline{\boldsymbol{C}}^{-1}/\partial\Delta\lambda_n$, (4) $\partial\|\overline{\boldsymbol{S}}\|_{\overline{\boldsymbol{a}}}/\partial\Delta\lambda_n$ and (5) $\partial\mathrm{Tr}\overline{\boldsymbol{S}}/\partial\Delta\lambda_n$in Eq. (A11) are given as follows:

(1) Using the hyperelastic constitutive law in Table 1, we obtain

$$\frac{\partial \overline{\boldsymbol{S}}}{\partial \Delta\lambda_n} = \frac{1}{2}\overline{\mathbb{C}} : \frac{\partial \overline{\boldsymbol{C}}}{\partial \Delta\lambda_n} + 2\kappa_1 J^{-2/3}\alpha_2\mathrm{DEV}\left[\frac{\partial \overline{\boldsymbol{A}}}{\partial \Delta\lambda_n}\right]. \tag{A12}$$

(2) By substituting Eq. (A8) into the expression

$$\frac{\partial \overline{\boldsymbol{A}}}{\partial \Delta\lambda_n} = \frac{\partial \overline{\boldsymbol{a}}}{\partial \Delta\lambda_n}\otimes\overline{\boldsymbol{a}} + \overline{\boldsymbol{a}}\otimes\frac{\partial \overline{\boldsymbol{a}}}{\partial \Delta\lambda_n}, \tag{A13}$$

$\partial\overline{\boldsymbol{A}}/\partial\Delta\lambda_n$ is obtained.

(3) By using Eq. (23) and the chain rule, $\partial\overline{\boldsymbol{C}}^{-1}/\partial\Delta\lambda_n$ is given as

$$\frac{\partial \overline{\boldsymbol{C}}^{-1}}{\partial \Delta\lambda_n} = -\mathbb{I}_{\overline{\boldsymbol{C}}^{-1}} : \frac{\partial \overline{\boldsymbol{C}}}{\partial \Delta\lambda_n} \tag{A14}$$

where the term $\partial\overline{\boldsymbol{C}}/\partial\Delta\lambda_n$is reported in Eq. (A9).

(4) Taking the derivative of $\|\overline{\boldsymbol{S}}\|_{\overline{\boldsymbol{a}}}$with respect to $\Delta\lambda_n$, we obtain

$$\frac{\partial \|\overline{\boldsymbol{S}}\|_{\overline{\boldsymbol{a}}}}{\partial \Delta\lambda_n} = 2\frac{\partial \overline{\boldsymbol{a}}}{\partial \Delta\lambda_n}\cdot(\overline{\boldsymbol{C}}\overline{\boldsymbol{S}}\overline{\boldsymbol{C}}\overline{\boldsymbol{a}}) + 2\overline{\boldsymbol{a}}\cdot\left(\frac{\partial \overline{\boldsymbol{C}}}{\partial \Delta\lambda_n}\overline{\boldsymbol{S}}\overline{\boldsymbol{C}}\overline{\boldsymbol{a}}\right) + \overline{\boldsymbol{a}}\cdot\left(\overline{\boldsymbol{C}}\frac{\partial \overline{\boldsymbol{S}}}{\partial \Delta\lambda_n}\overline{\boldsymbol{C}}\overline{\boldsymbol{a}}\right) \tag{A15}$$

in which $\partial\overline{\boldsymbol{a}}/\partial\Delta\lambda_n$, $\partial\overline{\boldsymbol{C}}/\partial\Delta\lambda_n$and $\partial\overline{\boldsymbol{S}}/\partial\Delta\lambda_n$ are shown in Eqs. (A8), (A9), and (A12), respectively.

(5) By taking the derivative of $\|\overline{\boldsymbol{S}}\|_{\overline{\boldsymbol{a}}}$with respect to $\Delta\lambda_n$, the expression of $\partial\mathrm{Tr}\overline{\boldsymbol{S}}/\partial\Delta\lambda_n$ is obtained as

$$\frac{\partial \mathrm{Tr}\overline{\boldsymbol{S}}}{\partial \Delta\lambda_n} = \frac{\partial \overline{\boldsymbol{S}}}{\partial \Delta\lambda_n} : \overline{\boldsymbol{C}} + \overline{\boldsymbol{S}} : \frac{\partial \overline{\boldsymbol{C}}}{\partial \Delta\lambda_n}. \tag{A16}$$

Substituting Eqs. (A12)–(A16) into Eq. (A11), the explicit expression of $\partial\bar{\boldsymbol{S}}^{DEV}/\partial\Delta\lambda_n$ is obtained. By using Eqs. (A6) and (A7), the expression of $\partial\bar{\boldsymbol{S}}^{DEV}/\partial\Delta\lambda_n$ together with Eqs. (A8) and (A9) leads to the explicit expression of $\partial\bar{J}_1/\partial\Delta\lambda_n$ and $\partial\bar{J}_2/\partial\Delta\lambda_n$. Consequently the explicit expression of $\partial\phi/\partial\Delta\lambda_n$ is obtained from Eq. (A4).

Appendix B: Estimation of model parameters by using the analytical solution of a simple model

The cell is treated as an isotropic closed cylindrical shell subjected to inner pressure P (turgor pressure). The small strain elasto-plastic deformation of a closed cylindrical shell has been fully studied in the literature (Lubliner, 1990). The stress distribution in the cylindrical part in a cylindrical coordinate system (r,θ,z) is

$$\sigma_r=-\tilde{P}\left(\frac{b^2}{r^2}-1\right),\quad \sigma_\theta=\tilde{P}\left(\frac{b^2}{r^2}+1\right),\quad \sigma_z=\tilde{P} \tag{B1}$$

where $\tilde{P}=P/(b^2/a^2-1)$, a and b are the inner radius and outer radius, respectively. By using Eqs. (38) and (B1) and setting $\boldsymbol{a}=\{a_r\quad a_\theta\quad a_z\}^T=\{0\quad 1\quad 0\}^T$, the spatial Spencer's deviatoric stress $\boldsymbol{\tau}^{dev}$ is calculated as

$$\boldsymbol{\tau}^{dev}=J\frac{\tilde{P}}{2}\frac{b^2}{r^2}\mathrm{Diag}[-1,0,1] \tag{B2}$$

where $\mathrm{Diag}[\cdot,\cdot,\cdot]$ denotes a diagonal tensor. By substituting Eq. (B2) into Eqs. (42) and (43), the two invariants of $\boldsymbol{\tau}^{dev}$ are given as

$$\tilde{J}_1=0,\quad \tilde{J}_2=J^2\frac{\tilde{P}^2}{2}\frac{b^4}{r^4}. \tag{B3}$$

As $\tilde{J}_1(=\bar{J}_1)$ vanishes, the quartic Eq. (55) degrades to a nontrivial quadratic format as

$$(1+h)(\theta-Y_2^2)^2-\tilde{J}_2Y_2^2=0. \tag{B4}$$

Solving Eq. (B4) we obtain θ. By substituting θ and Eq. (B3) into Eq. (55), the overstress function ($m=1$) is obtained as

$$\bar{\phi}_{dev}=\sqrt{\tilde{J}_2}-(1+h)Y_2. \tag{B5}$$

By using Eqs. (B3), (B5), and (68), a direct calculation of $\partial\bar{\phi}/\partial\boldsymbol{\tau}$ gives the plastic flow direction as

$$\mathrm{sym}\boldsymbol{R}^*=\frac{\partial\bar{\phi}_{dev}}{\partial\boldsymbol{\tau}}=\frac{1}{\sqrt{\tilde{J}_2}}\boldsymbol{\tau}^{dev}=\frac{1}{\sqrt{2}}\mathrm{Diag}[-1,0,1]. \tag{B6}$$

Let $\mathrm{sym}\boldsymbol{R}^*=\mathrm{sym}\bar{\boldsymbol{R}}^*$ in small strain. By substituting Eqs. (B5) and (B6) into Eq. (63) and (77) and taking $\dot{\lambda}_{vol}=\dot{\lambda}_{\boldsymbol{a}}=0$, the plastic strain rate is obtained as

$$\boldsymbol{D}^g=\bar{\boldsymbol{D}}^g=\frac{\sqrt{\tilde{J}_2}-(1+h)Y_2}{\sqrt{2}\eta}\mathrm{Diag}[-1,0,1]. \tag{B7}$$

Thus the longitudinal plastic strain rate, i.e. rate of elongation of cell wall, is

$$D_z^g=\left(\sqrt{\tilde{J}_2}-(1+h)Y_2\right)\Big/\sqrt{2}\eta. \tag{B8}$$

The viscoplastic parameters of the model can be estimated from Eq. (B8), as generally the data of elongation of cell wall are the only kind of data available. If data of an experimental data involving a change of turgor pressure P is available, the following estimation of parameters can be carried out. Given two rates of elongation, e.g. $D^g_{z\langle 1\rangle}$ and $D^g_{z\langle 2\rangle}$, under two different turgor pressures, $P_{\langle 1\rangle}$ and $P_{\langle 2\rangle}$, the parameters of viscoplasticity can be obtained by using Eq. (B8) as

$$(1+h)Y_2=\frac{\sqrt{\tilde{J}_{2\langle 1\rangle}}-(D^g_{z\langle 1\rangle}/D^g_{z\langle 2\rangle})\sqrt{\tilde{J}_{2\langle 2\rangle}}}{1-(D^g_{z\langle 1\rangle}/D^g_{z\langle 2\rangle})},\quad \eta=(\sqrt{\tilde{J}_{2\langle 1\rangle}}-(1+h)Y_2)/\sqrt{2}D^g_{z\langle 1\rangle}. \tag{B9}$$

It is noted that the dynamic yield threshold, $(1+h)Y_2$, can be estimated by this method. Besides the viscoplastic parameters, Young's modulus E can be estimated from the instantaneous response of elongation to the change of turgor pressure.

References

Baskin, T.I., 2005. Anisotropic expansion of the plant cell wall. Annu. Rev. Cell Dev. Biol. 21, 203–222.
Beckman, C.H., 1971. The plasticizing of plant cell walls and tylose formation-a model. Physiol. Plant Pathol. 1, l–10.
Belytschko, T., Liu, W.K., Moran, B., 2001. Nonlinear Finite Elements for Continua and Structures. John Wiley & Sons, Chichester.
Boudaoud, A., 2003. Growth of walled cells: from shells to vesicles. Phys. Rev. Lett. 91, 018104.
Bruce, D.M., 2003. Mathematical modelling of the cellular mechanics of plants. Phil. Trans. R. Soc. Lond. B 358, 1437–1444.
Burgert, I., Fratzl, P., 2007. Mechanics of the expanding cell wall. In: Verbelen, J.-P., Vissenberg, K. (Eds.), The Expanding Cell, Springer, Berlin, pp. 191–216.

Chaplain, M.A.J., 1993. The strain energy function of an ideal plant cell wall. J. Theor. Biol. 163, 77–97.
Chuong, C.J., Fung, Y.C., 1986a. Residual stress in arteries. In: Schmid-Schonbein, G.W., Woo, S.L.-Y., Zweifach, B.W. (Eds.), Frontiers in Biomechanics, Springer, New York, pp. 117–129.
Chuong, C.J., Fung, Y.C., 1986b. On residual stresses in arteries. J. Biomech. Eng. 108, 189–192.
Cosgrove, D.J., 1986. Biophysical control of plant cell growth. Annu. Rev. Plant Physiol. 37, 377–405.
Cosgrove, D.J., 1987. Wall relaxation and the driving forces for cell expansive growth. Plant Physiol. 84, 561–564.
Cosgrove, D.J., 1993a. How do plant cell walls extend? Plant Physiol 102, 1–6.
Cosgrove, D.J., 1993b. Wall extensibility: its nature, measurement and relationship to plant cell growth. New Phytol. 124, 1–23.
Cosgrove, D.J., 1997. Assembly and enlargement of the primary cell wall in plants. Annu. Rev. Cell Dev. Biol. 13, 171–201.
Cosgrove, D.J., 2000. Expansive growth of plant cell walls. Plant Physiol. Biochem. 38, 109–124.
Cosgrove, D.J., 2001. Wall structure and wall loosening. a look backwards and forwards. Plant Physiol. 125, 131–134.
Cowin, S.C., 2004. Tissue growth and remodeling. Annu. Rev. Biomed. Eng. 6, 77–107.
Derbyshire, P., Findlay, K., Maureen, C., McCann, M.C., Roberts, K., 2007. Cell elongation in Arabidopsis hypocotyls involves dynamic changes in cell wall thickness. J. Exp. Bot. 58, 2079–2089.
Dumais, J., 2007. Can mechanics control pattern formation in plants? Curr Opinion Plant Biol. 10, 58–62.
Dumais, J., Shaw, S.L., Steele, C.R., Long, S.R., Ray, P.M., 2006. An anisotropic-viscoplastic model of plant cell morphogenesis by tip growth. Int. J. Dev. Biol. 50, 209–222.
Dumais, J., Steele, C.R., 2000. New evidence for the role of mechanical forces in the shoot apical meristem. J. Plant Growth Regul. 19, 7–18.
Dyson, R.J., Jensen, O.E., 2010. A fibre-reinforced fluid model of anisotropic plant cell growth. J. Fluid Mech. 655, 472–503.
Epstein, M., Maugin, G.A., 1996. On the geometrical structure of anelasticity. Acta Mech. 115, 119–131.
Epstein, M., Maugin, G.A., 2000. Thermomechanics of volumetric growth in uniform bodies. Int. J. Plasticity 16, 951–978.
Fung, Y.C., 1990. Biomechanics: Motion, Flow, Stress, and Growth. Springer, New York.
Gao, H., Ji, B., Jager, I.L., Arzt, E., Fratzl, P., 2003. Materials become insensitive to flaws at nanoscale: lessons from nature. Proc. Natl. Acad. Sci. USA 100, 5597–5600.
Garikipati, K., Arruda, E.M., Grosh, K., Narayanan, H., Calve, S., 2004. A continuum treatment of growth in biological tissue the coupling of mass transport and mechanics. J. Mech. Phys. Solids 52, 1595–1625.
Gasser, T.C., Ogden, R.W., Holzapfel, G.A., 2006. Hyperelastic modelling of arterial layers with distributed collagen fibre orientations. J. R. Soc. Interface 3, 15–35.
Geitmann, A., Ortega, J.K.E., 2009. Mechanics and modelling of plant cell growth. Trends Plant Sci. 14, 467–478.
Green, P.B., Erickson, R.O., Buggy, J., 1971. Metabolic and physical control of cell elongation rate. In vivo studies in Nitella. Plant Physiol. 47, 423–430.
Hamant, O., Traas, J., 2009. The mechanics behind plant development. New Phytol. 185, 369–385.
Hamant, O., Heisler, M.G., Jönsson, H., Krupinski, P., Uyttewaal, M., Bokov, P., Corson, F., Sahlin, P., Boudaoud, A., Meyerowitz, E.M., Couder, Y., Traas, J., 2008. Developmental patterning by mechanical signals in Arabidopsis. Science 322, 1650–1655.
Hettiaratchi, D.R.P., O'callagham, J.R., 1978. Structural mechanics of plant cells. J. Theor. Biol. 74, 235–257.
Imatani, S., Maugin, G.A., 2002. A constitutive model for material growth and its application to three-dimensional finite element analysis. Mech. Res. Commun. 29, 477–483.
Iwamoto, S., Kai, W., Isogai, A., Iwata, T., 2009. Elastic modulus of single cellulose microfibrils from tunicate measured by atomic force microscopy. Biomacromolecules 10, 2571–2576.
Keckes, J., Burgert, I., Fruhmann, K., Muller, M., Kolln, K., Hamilton, M., Burghammer, M., Roth, S.V., Stanzl-Tschegg, S., Fratzl, P., 2003. Cell-wall recovery after irreversible deformation of wood. Nat. Mater. 2, 810–814.
Kerstens, S., Decraemer, W.F., Verbelen, J.-P., 2001. Cell walls at the plant surface behave mechanically like fibre-reinforced composite materials. Plant Physiol. 127, 381–385.
Kutschera, U., 1990. Cell-wall synthesis and elongation growth in hypocotyls of *Helianthus annuus*. L. Planta 181, 316–323.
Lockhart, J.A., 1965a. An analysis of irreversible plant cell elongation. J. Theor. Biol. 8, 264–275.
Lockhart, J.A., 1965b. Cell extension. In: Bonner, J., Varner, J.E. (Eds.), Plant Biochemistry, Academic Press, New York, pp. 827–849.
Lubarda, V.A., 2004. Constitutive theories based on the multiplicative decomposition of deformation gradient: thermoelasticity, elastoplasticity, and biomechanics. Appl. Mech. Rev. 57, 95–108.
Lubliner, J., 1990. Plasticity Theory. Macmillan, New York.
Mandel, J., 1971. Plasticité Classique et Viscoplasticité (CISM Lecture Notes, Udine, Italy). Springer-Verlag, Vienna.
Marga, F., Grandbois, M., Cosgrove, D.J., Baskin, T.I., 2005. Cell wall extension results in the coordinate separation of parallel microfibrils: evidence from scanning electron microscopy and atomic force microscopy. Plant J. 43, 181–190.
Marsden, J.E., Hughes, T.J.R., 1994. Mathematical Foundation of Elasticity. Dover, NewYork.
Maugin, G.A., 1999. The Thermomechanics of Nonlinear Irreversible Behaviours. World Scientific Publishing Ltd, Singapore.
Maugin, G.A., 2011. Configurational Forces: Thermo-Mechanics, Physics, Mathematics and Numerics. CRC Press, Boca Raton.
McCann, M.C., Wells, B., Roberts, K., 1990. Direct visualization of cross-links in the primary plant cell wall. J. Cell Sci. 96, 323–334.
Moran, B., Ortiz, M., Shih, C.F., 1990. Formulation of implicit finite element methods for multiplicative finite deformation plasticity. Int. J. Numer. Methods Eng. 29, 483–514.
Ortega, J.K.E., 1990. Governing equations for plant cell growth. Physiol. Planta 79, 116–121.
Pietruszka, M., 2009. General proof of the validity of a new tensor equation of plant growth. J. Theor. Biol. 256, 584–585.
Piggott, M.R., 1980. Load Bearing Fibre Composites. Pergamon Press, Oxford.
Proseus, T.E., Boyer, J.S., 2005. Turgor pressure moves polysaccharides into growing cell walls of *Chara coralline*. Ann. Bot. 95, 967–979.
Proseus, T.E., Boyer, J.S., 2006. Identifying cytoplasmic input to the cell wall of growing *Chara coralline*. J. Exp. Bot. 57, 3231–3242.
Proseus, T.E., Boyer, J.S., 2007. Tension required for pectate chemistry to control growth in *Chara coralline*. J. Exp. Bot. 58, 4283–4292.
Proseus, T.E., Ortega, J.K.E., Boyer, J.S., 1999. Separating growth from elastic deformation during cell enlargement. Plant Physiol. 119, 775–784.
Proseus, T.E., Zhu, G.-L., Boyer, J.S., 2000. Turgor, temperature and the growth of plant cells using *Chara corallina* as a model system. J. Exp. Bot. 51, 1481–1494.
Ray, P.M., Green, P.B., Cleland, R., 1972. Role of turgor in plant cell growth. Nature 239, 163–164.
Refregier, G., Pelletier, S., Jaillard, D., Hofte, H., 2004. Interaction between wall deposition and cell elongation in dark-grown hypocotyl cells in Arabidopsis. Plant Physiol. 135, 959–968.
Roberts, K., 1994. The plant extracellular matrix: in a new expansive mood. Curr. Opinion Cell Biol. 6, 688–694.
Rodriguez, E.K., Hoger, A., McCulloch, A., 1994. Stress-dependent finite growth in soft elastic tissue. J. Biomech. 27, 455–467.
Schopfer, P., 2006. Biomechanics of plant growth. Am. J. Bot. 93, 1415–1425.
Simo, J.C., Hughes, T.J.R., 1998. Computational Inelasticity. Springer, New York.
Simo, J.C., Ortiz, M., 1985. A unified approach to finite deformation elastoplastic analysis based on the use of hyperelastic constitutive equations. Comput. Methods Appl. Mech. Eng. 49, 221–245.
Skalak, R., 1981. Growth as a finite displacement field. In: Carlson, D.E., Shield, R.T. (Eds.), Proceedings off the IUTAM Symposium on Finite Elasticity, Martinus Nijhoff Publishers, The Hague, pp. 347–355.
Spatz, H.-C., Kohler, L., Niklas, K.J., 1999. Mechanical behaviour of plant tissues: composite materials or structures? J Exp. Biol. 202, 3269–3272.
Spencer, A.J.M., 2001. A theory of viscoplasticity for fabric-reinforced composites. J. Mech. Phys. Solids 49, 2667–2687.

Stamenovic, D., Ingber, D.E., 2009. Tensegrity-guided self assembly from molecules to living cells. Soft Matter 5, 1137–1145.
Steele, C.R., 2000. Shell stability related to pattern formation in plants. J. Appl. Mech. 67, 237–247.
Suslov, D., Verbelen, J.-P., 2006. Cellulose orientation determines mechanical anisotropy in onion epidermis cell walls. J. Exp. Bot. 57, 2183–2192.
Taber, L.A., 1995. Biomechanics of growth, remodelling, and morphogenesis. Appl. Mech. Rev. 48, 488–545.
Taiz, L., 1984. Plant cell expansion: regulation of cell wall mechanical properties. Annu. Rev. Plant Physiol. 35, 585–657.
Toole, G.A., Gunning, P.A., Parker, M.L., Smith, A.C., Waldron, K.W., 2001. Fracture mechanics of the cell wall of *Chara coralline*. Planta 212, 606–611.
Treloar, L.R.G., 2005. In: The Physics of Rubber ElasticityThird edition Clarendon Press, Oxford.
Verbelen, J.-P., Vissenberg, K., 2007. Cell expansion: Past, present and perspectives. In: Verbelen, J.-P., Vissenberg, K. (Eds.), The Expanding Cell, Springer, Berlin, pp. 1–6.
Veytsman, B.A., Cosgrove, D.J., 1998. A model of cell wall expansion based on thermodynamics of polymer networks. Biophys. J. 75, 2240–2250.
Zhu, G.L., Boyer, J.S., 1992. Enlargement in Chara studied with a turgor clamp. Plant Physiol. 100, 2071–2080.